AFRISCAT

FINAL REPORT

ESA CONTRACT N°4000111758/14/NL/FF/GP

Prepared by	CESBIO Team (T. Le Toan, L. Villard, T. Koleck, A. Hamadi) ONERA Team (P. Borderies) POLIMI Team (S. Tebaldini) CMCC team (G. Nicolini, G. Vaglio Laurin)	
Approved by	Thierry Koleck (CESBIO)	Date and signature 30/04/18

DOCUMENT INFORMATION

Document Title: AfriScat Final Report
Keyword :BIOMASS, AfriScat, Campaign
Contributors : ONERA Team (P. Borderies) CESBIO Team (L. Villard, A. Hamadi, T. Koleck) CMCC Team (G. Nicolini)
Summary : This document summarizes the work done during the Afriscat experiment in Ghana

DOCUMENT CHANGES

Issue	Date	Changes	Comments
1	30/04/18		

REFERENCE DOCUMENTS:

RD 1: Statement of Work, Appendix 1 to RFP 14.572, “Technical Assistance For The Deployment Of Tower-based Radar and Geophysical Measurements during the Afriscat Experiment”, ref EOP-SM/2616/RB-rb

RD 2: Afriscat Implementation Plan, ref : DCT/SI/AR/14-19620

RD 3 : Afriscat Hardware Refurbishment Report, ref : DCT/SI/AR 2014.0017322

RD 4: CCN 2 to Afriscat ESTEC Contract 4000111758/NL/FF/gp, ref EOP-SM/2386

SUMMARY

1. INTRODUCTION

The retrieval algorithms currently developed for BIOMASS are based on the use of P-band intensity, interferometry and tomography. The last two techniques require high temporal coherence for coherent processing of data from repeat pass acquisitions. The condition to have exploitable interferometric or tomographic information is to have high temporal coherence over forests for time intervals compatible with the BIOMASS mission. This requirement is particularly important for tropical forests for which interferometric (Pol-InSAR and TomoSAR) measurements can efficiently complement polarimetric data.
Initially, temporal coherence has been addressed during the TropiSAR experiment, over a dense tropical forest in French Guiana, during which multi-temporal acquisitions during a 20 days period have been performed in August 2009. Later, a better characterization of temporal variations of backscattering in a full range of seasons and weather conditions has been done in the TropiSCAT campaign [1]. A tower-based scatterometer has been developed and deployed at the Paracou field station, which is the same site investigated during the TropiSAR campaign.

In 2015, ESA and CNES decided to support a new experiment, based on the TropiSCAT experience, to acquire long-term P-Band radar data in an African tropical forest.

As for TropiSCAT, the major objectives of the experiment are the temporal survey of the variation of the measurements in time scales ranging from diurnal, weekly, monthly, up to 12 months of observation. The measurements which have to be tracked are in order of priority:

- The temporal coherence in HH, VV and HV polarizations, at a very short rate in the order of 15 minutes, covering daily and monthly scale,

- The backscattering coefficient at HH, VV and HV polarizations and in all time scales,

- 2D vertical imaging through tomographic focusing;

- The vertical distribution of temporal coherence, as obtained by comparing tomographic data taken at different times, covering time scales of minutes, days, and months.

In addition to electromagnetic scattering measurements, ancillary in-situ data are also collected on the same area.

2. ANKSA SITE DESCRIPTION

The site selected to host Afriscat experiment was the Ankasa Forest Conservation Area, Ghana:

- Area : 509 km2
- Pristine forest with about 800 species
- 4-5 vegetation layer max 30-35 m
- Bimodal rain distribution: April-June and September-November
- Average annual rain 1700-2000 mm
- Average monthly temperature 24 - 28 °C
- Average humidity 75 – 90%
- Soil: Oxysols (pH 3.5 - 4.0)
- Site coordinates: 5.26854275 (lat); -2.69420592 (long)

Figure 1 - Location and picture of Ankasa tower

3. CAMPAIGN PREPARATION

The first phase of the campaign activity was related to the definition, the building and the installation of the Afriscat instrument.

3.1.EXPERIMENT DEFINITION

AfriSCAT experiment was defined as a follower of TropiSCAT [1]. The instrument concept was kept as is. Only technical implementation was changed to fit to the new site and to improve the reliability.

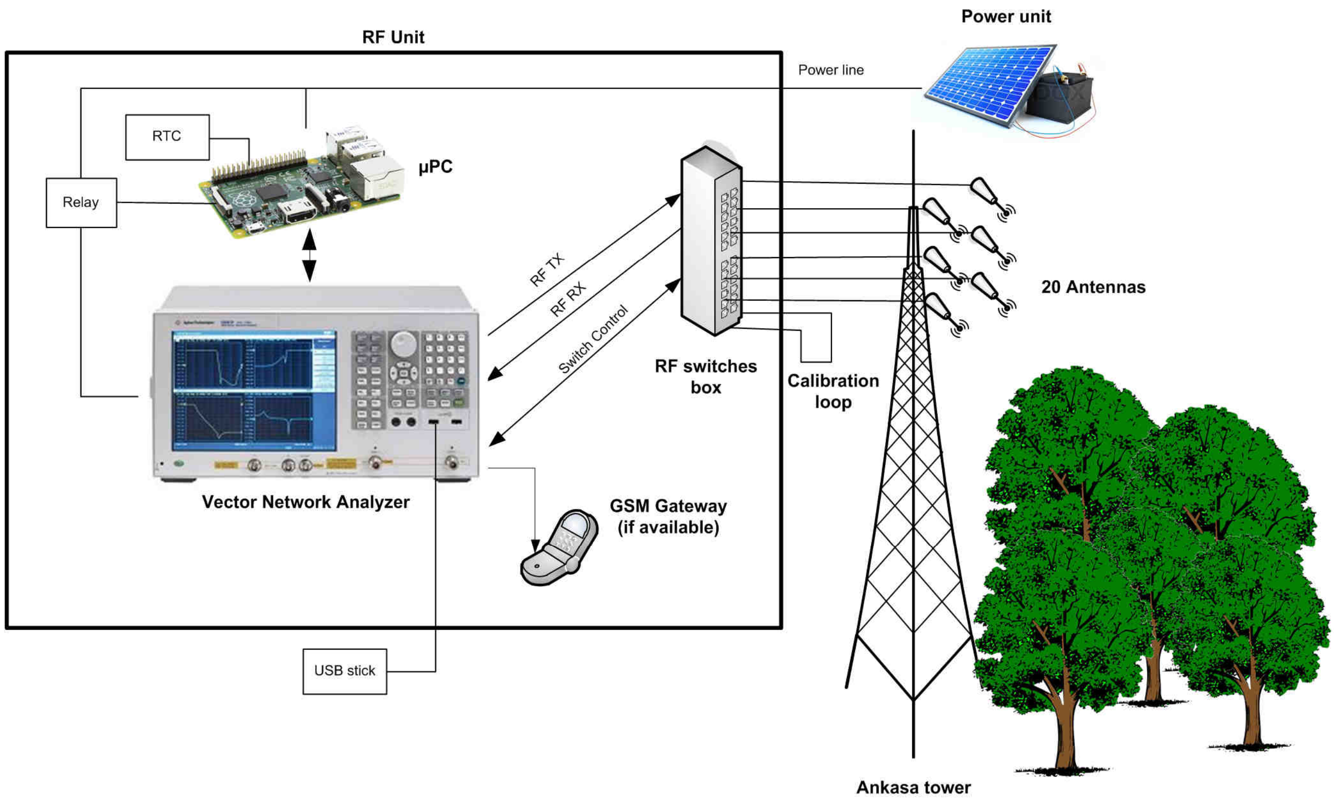

Figure 2 - Synoptic of theAfriScat instrument

As shown on Figure 2, the instrument is composed of a VNA (Vector Network Analyzer), a set of wide-band antennas, a radio frequency (RF) switching device and a command unit.

The VNA works as a transmitter/receiver (RX/TX) device. So it has been configured in S21 mode (port 1 in TX, port 2 in RX).

The VNA generates a RF signal, over a 200 MHz frequency band. This signal travels in a low-loss cable to the RF switch box, which routes the signal to the selected TX antenna. This antenna radiates to the forest. Then the backscattered signal is received by the selected RX antenna and driven to the VNA via a second low-loss cable. The VNA records the S21 parameter over the frequency band.

An array of 20 antennas has been designed to fulfill the requirements for the tomography acquisitions. This design had to deal with mechanical and electrical constraints due to the antenna type (log-periodic antennas): the inter antenna coupling must be minimized and the TX and RX antennas must be separated. The final antenna array design is shown on Figure 3. It is identical to TropiSCAT one.

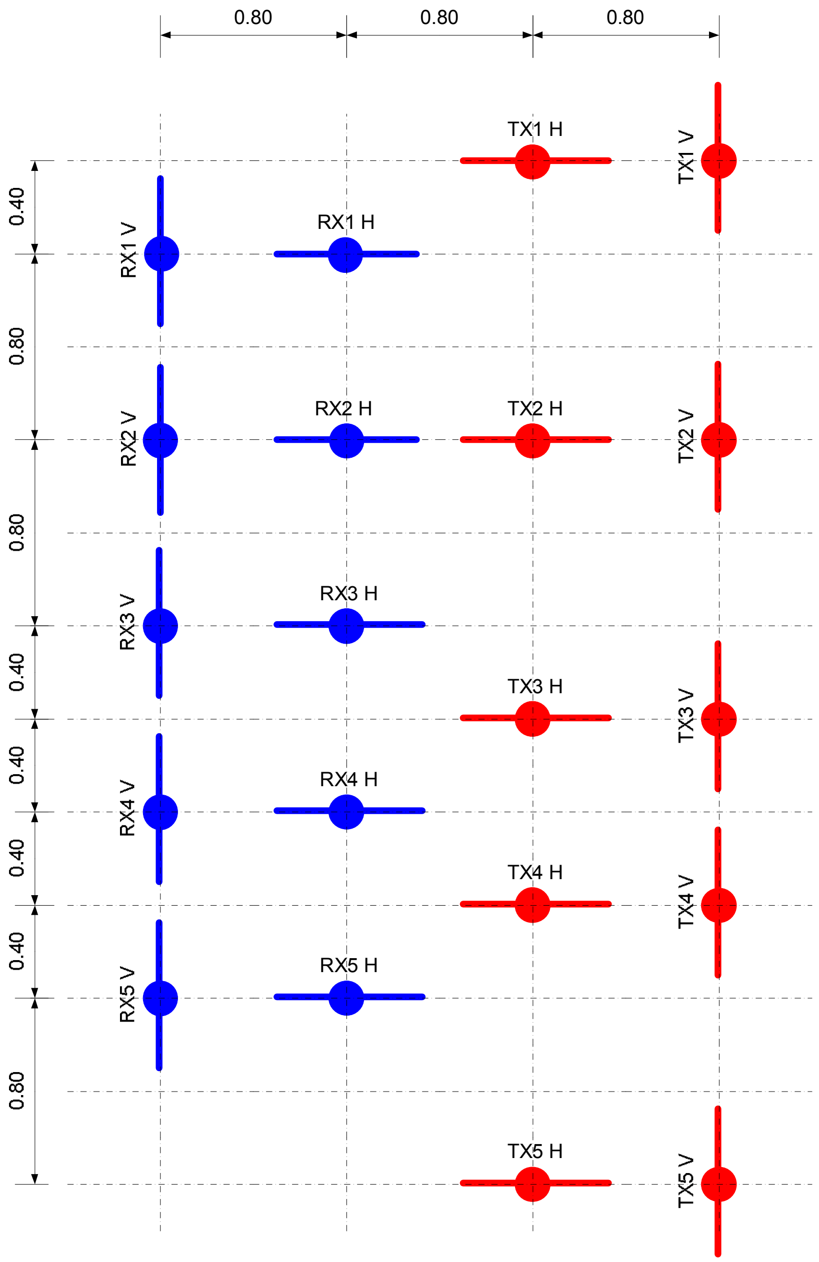

Figure 3 - Geometry of the antenna array

The definition of the experiment has taken into account the environment where the instrument is deployed. The main constraints we have to deal with were:

- The tropical climatic conditions (temperature, humidity, sun)
- The limited electrical power available and its potentially poor quality
- The autonomy of the instrument because of the lack of remote control capability
- Maximum reuse of TropiScat hardware to keep the cost reasonnable.

Considering all these constraints, we decided the following changes compared to Tropiscat instrument design:

- Hardware will be placed on the tower top
  - Avantages:
    - shorter RF cables
    - lower surrounding humidity
  - Disavantages:
    - need a weather-proof box for hardware protection, from rain and sun radiation
    - more difficult maintenance operation
    - more difficult data collecting
- Improvement of sensible components
  - To avoid problems encountered during the Tropiscat campaign, we:
    - selected more resistant RF cables
    - changed the RF switches by more robust ones. The command circuit was also upgraded to detect switche failure.

On Ankasa site, electrical was only provided by solar panel located on the tower top. As the surface of solar panel was limited to few meters square, the available power was very limited.

To deal with this constraint, we needed to switch on the instrument only for few hours per day. So, the instrument must be able to switch on/off automatically at programmed time. Figure 4 illustrates the electrical architecture of the instrument.

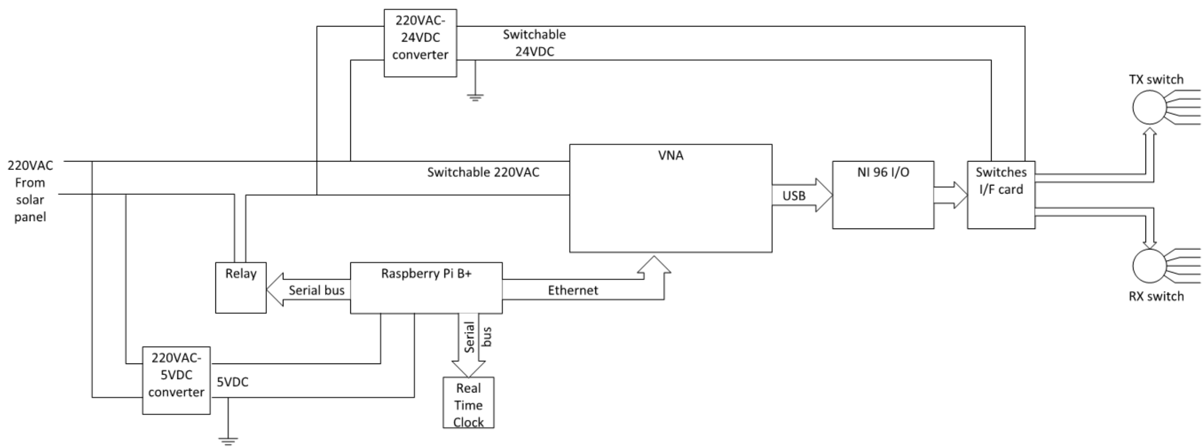

Figure 4 - Instrument electrical architecture

The Raspberry Pi, associated to a real time clock is in charge of the power management. It was in charge of switching on/off the 220 VAC line for the VNA.

The VNA was programmed to start automatically the acquisitions when it is powered on.

When switch-off time arises, the Raspberry Pi power-off the VNA by software and switch off the power line few minutes later.

3.2. HARDWARE REFURBISHING AND INSTRUMENT INTEGRATION

To reduce the cost of the experiment, we reused the TropiScat hardware. A refurbishment step was necessary to repair and check all devices.

3.2.1. AGILENT E6051B VECTOR NETWORK ANALYZER

The VNA is the same Agilent E6051B from TropiScat. After being in French Guiana for 3 years, it was refurbished by the manufacturer to replace the damaged parts (hard disk and main motherboard) and factory-calibrated.

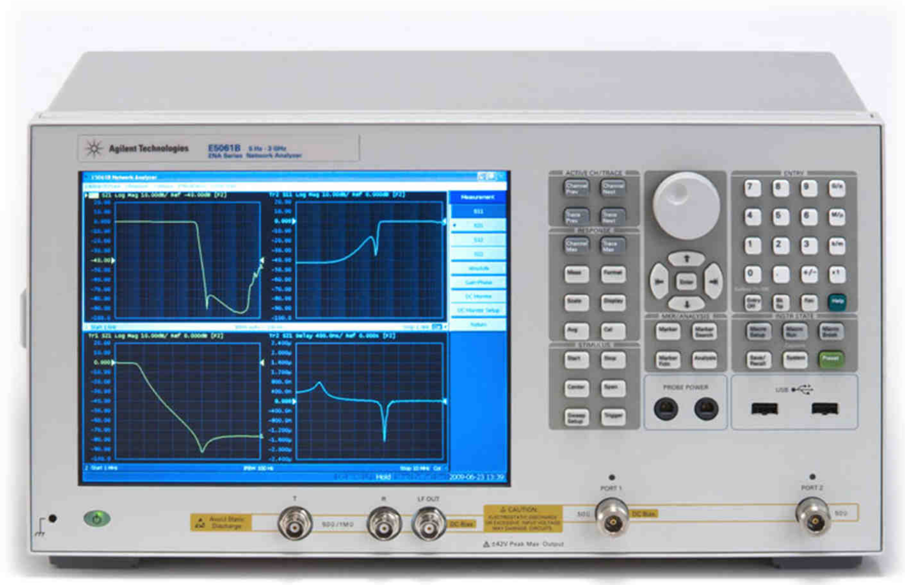

Characteristics and performances are given here: https://www.keysight.com/en/pdx-x201771-pn-E5061B/ena-vector-network-analyzer?cc=FR&lc=fre

3.2.2. ANTENNAS

All antennas have been reused from the Tropiscat experiment. Theses antenna are LP400 model from Satimo manufacturer.

They have been checked in an acechoic chamber, both in SWVR and gain. Four antennas needed to be repaired.

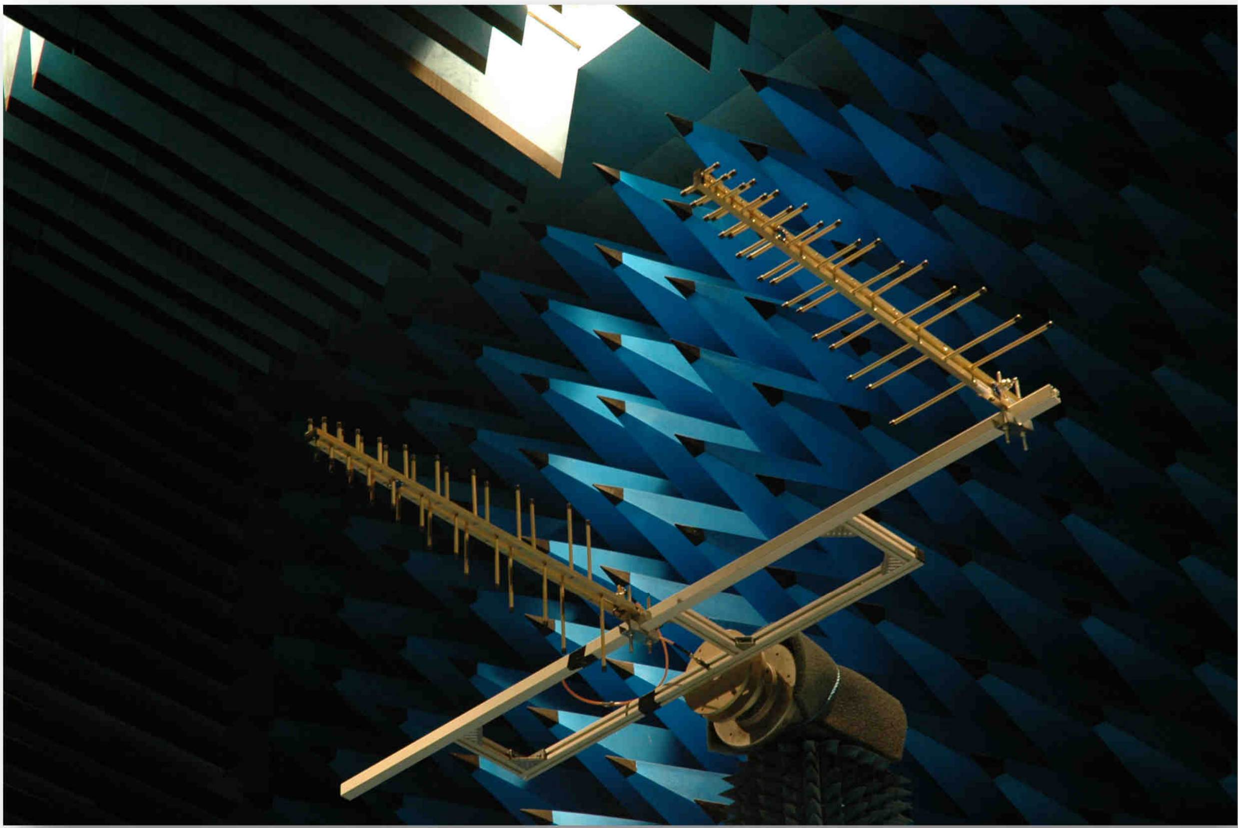

Figure 5 - LP400 log-periodic antenna

3.2.3. RF SWITCHES

Considering the experience from Tropiscat, the switch boxes have been completely re-designed to improve the reliability. We used two Radiall SP12T electromechanical switches. These switches allow:

- direct addressing the 10 antennas (no need two-stages switches)
- driving by TTL-level signal (5V)
- true position checking

Figure 6 - Radial SP12T switch

The VNA is connected to the antennas through two SP12T switches, one for transmitting (TX) and one for receiving (RX).

The switches have been connected as shown on Figure 7:

- 10 ports connected to the antennas
- 1 port connected to a long cable, identical to the cables used for antenna feeding. This line (called calibration loop) is use for VNA calibration purpose.
- 1 port connected directly the two switches without passing thru a cable (called short loop). This line is used to check the system stability.

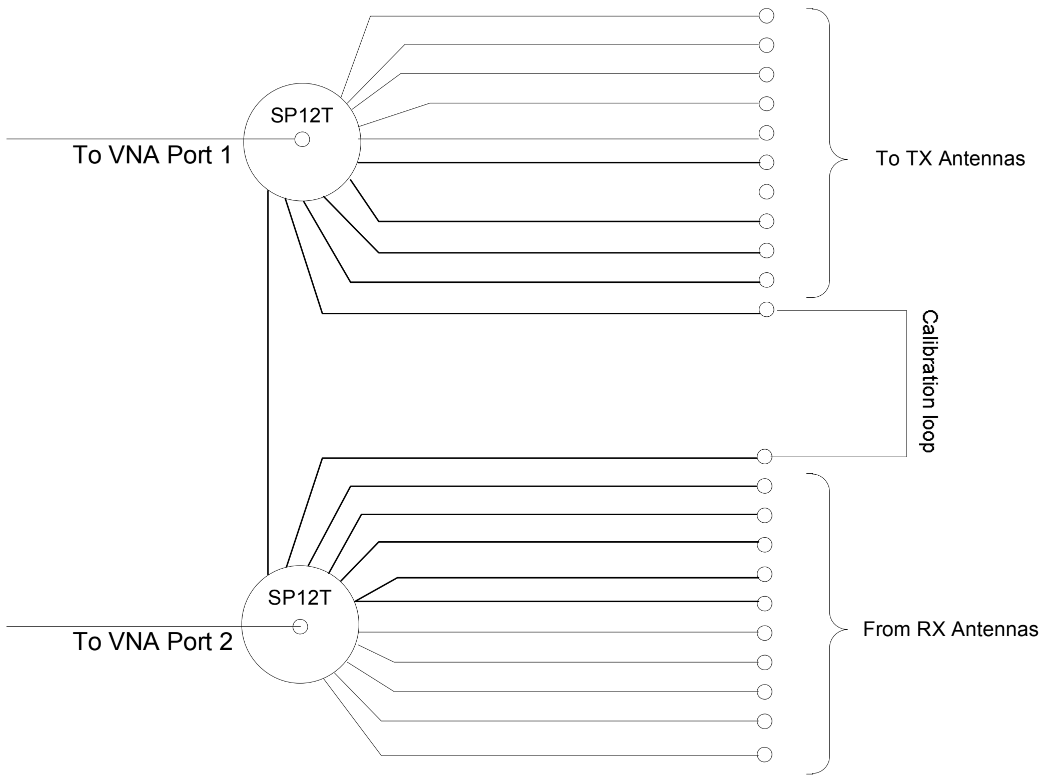

Figure 7 - RF Switches architecture

3.2.4. LOW-LOSS CABLES

6 meters long low-loss cables were used to feed the antennas. The calibration loop was build by connecting two cables, in order to have the same electrical length as for antennas.

All cables was covered by an additional sheath for sun protection.

Figure 8 - RF cables for antennas

3.2.5. INSTRUMENT TESTING

Before packging and shipping to Ghana, the complete antenna array was built in ONERA facility. Functionnal tests (Figure 9) have been done to ensure the well functioning of all parts.

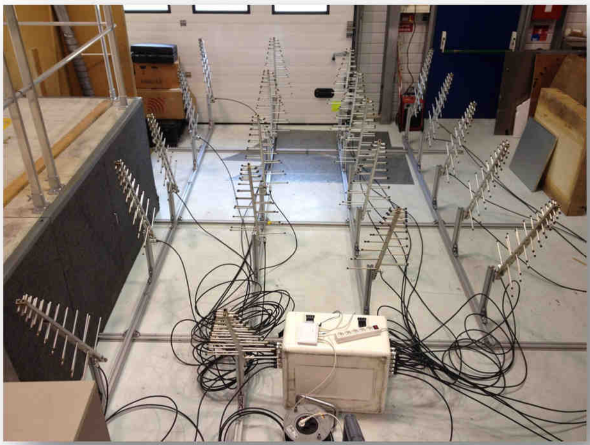

Figure 9 – Antenna array and instrument test in ONERA facility

3.3.EXPERIMENT SETUP AND TESTS

All hardware, including batteries for the power generation unit was sent in Ghana in March 2015. After a week of negociation with custom authorities, the package arrived safely to Ankasa.

A first check up was successfully done on the instrument before the setup on the tower.

The installation consisted in the following steps:

- Installing the metallic structure to support the antenna array
- Installation and pointing the antennas
- Installation of additional solar panels and batteries
- Installation of instrument
- Functionnal tests

Figure 10 – Instrument setup on the tower

3.3.1. ANALYSE OF IMPULSE RESPONSES

The first tests were dedicated to the checking of the impulse responses of the system i.e. the responses of the system in the time domain.

Next figures show typical examples of impulse responses of the forest for the 3 polarizations: HH in Figure 11, VV in Figure 12 and HV in Figure 13. First, one can see that the result is as expected. In the very low range (few meters) the direct coupling between the two considered antennas is clearly present. Then the tower echo is obvious as decreasing lobes. It may include some resonances between the antennas of the array themselves and interactions with the tower. Afterwards at approximately 25 m range the part of the forest closest to the antennas begins to appear with contribution of the volume part of the forest only. Beyond the complete forest is seen by the radar.

On the graphs, it can be checked that at 25 m the tower contribution is more than 10 dB below the first significant echoes of the forest and looking at its decaying behavior one can see that the tower echo contribute insignificantly to the foliage only response, and the full forest is free of tower contribution.

It is to note that since at Ankasa the forest fully surrounds the tower so that the dip between the tower echo and the foliage beginning is less deep than for Tropiscat. It is to note also that the range to which the canopy contribution appears is 25 meters whereas for Tropiscat is around 30 meters, for the same reason.

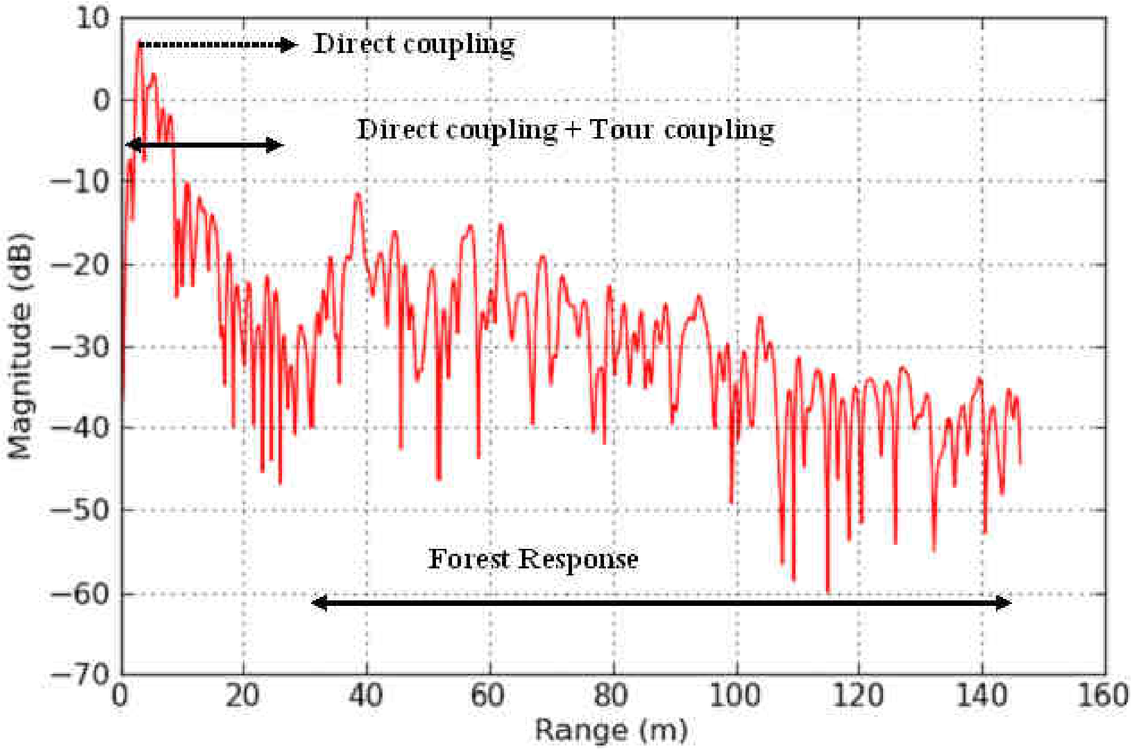

Figure 11: Example of forest raw impulse response : HH polarisation

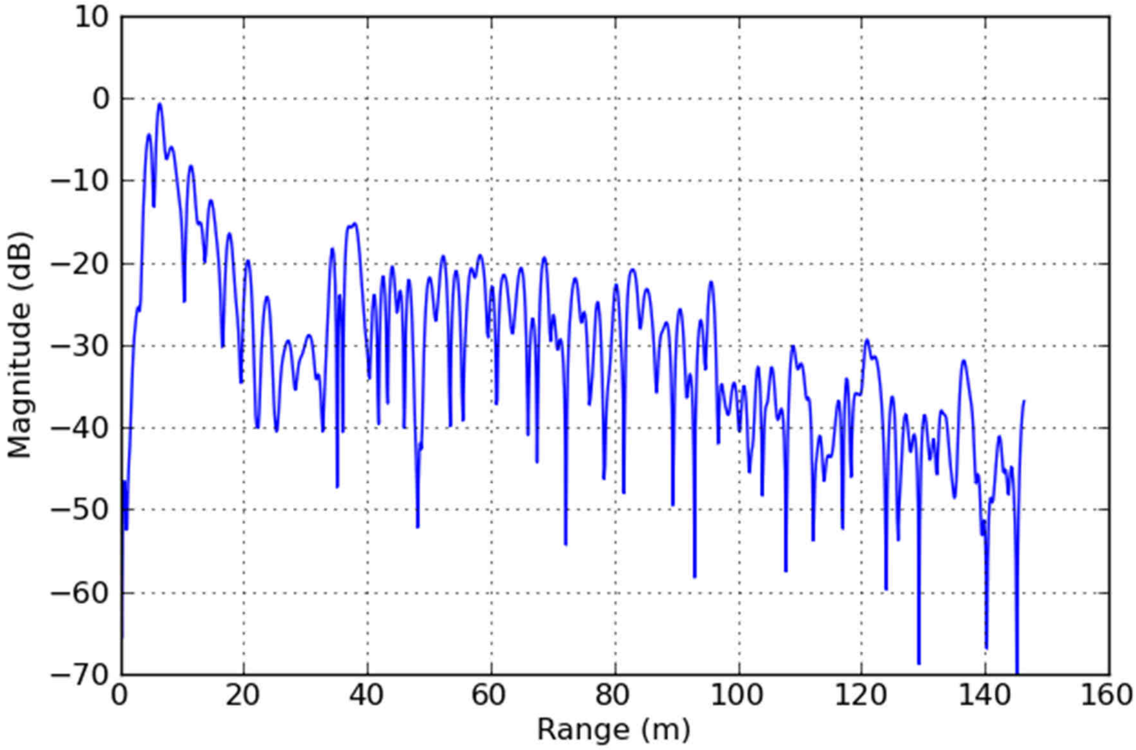

Figure 12: Example of forest raw impulse response: VV polarisation

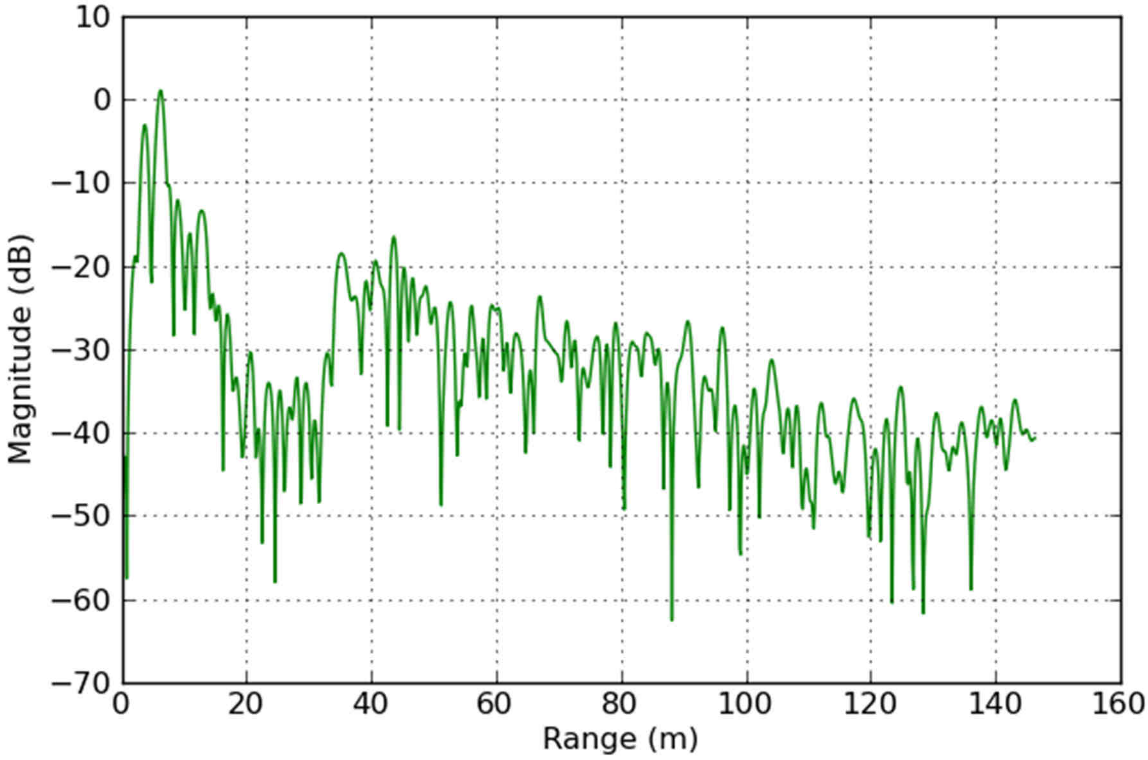

Figure 13 : Example of forest raw impulse response: HV polarization

Some measurements have been done with a corner reflector (CR) on ground. However this operation was here rather difficult because the forest starts just at the tower bottom. Fortunately we could find a location on forest ground where optically the path to the antennas is relatively free of foliage interception. This location is at 30 m distance from the tower which means 62.6 meters range from an antenna couple phase center located at 55 meters height.

The forest with CR embedded was measured on the 26th of February 2016 at 5 pm and the forest alone, with CR displaced and reoriented so that it is no more a strong diffracting point, 10 minutes later. The CR was located at 30 m distance from the tower. Note that the CR is not perfect and due to the constraint of the possibility of locating it inside the forest its dimensions are limited (we have approximately edge 1.8 meter long). Figure 14 represents the forest impulse response with the corner reflector embedded (HH polarization) for the whole set of antennas pairs. In this plot, the abscissa still represents the distance the range to the antennas. We retrieve the behavior described formerly with the tower part, followed by the canopy only part and finally the full forest. We can observe a peak at around 62 meters (in range) that corresponds to the corner reflector response. Actually, its level does not overlap strongly the average surrounding forest and it is weaker than the ground nadir echo located at 55 meters range. Figure 14 represent the same scene with forest removing with complex subtraction of the forest 10 minutes later. Now the peak corresponding to the CR range is more clearly visible and the nadir echo is removed. Note also that up to 30 meters the backscattering is strongly damped due to the coherent nature of the tower echo. This experiment is a proof of the well functioning of the system for all the antenna pairs with in particular the phase stability which lets remove the coherent echoes and the nadir echo. Nevertheless, with or without chamber correction, the forest level remains close in average which is due the changes in the forest.

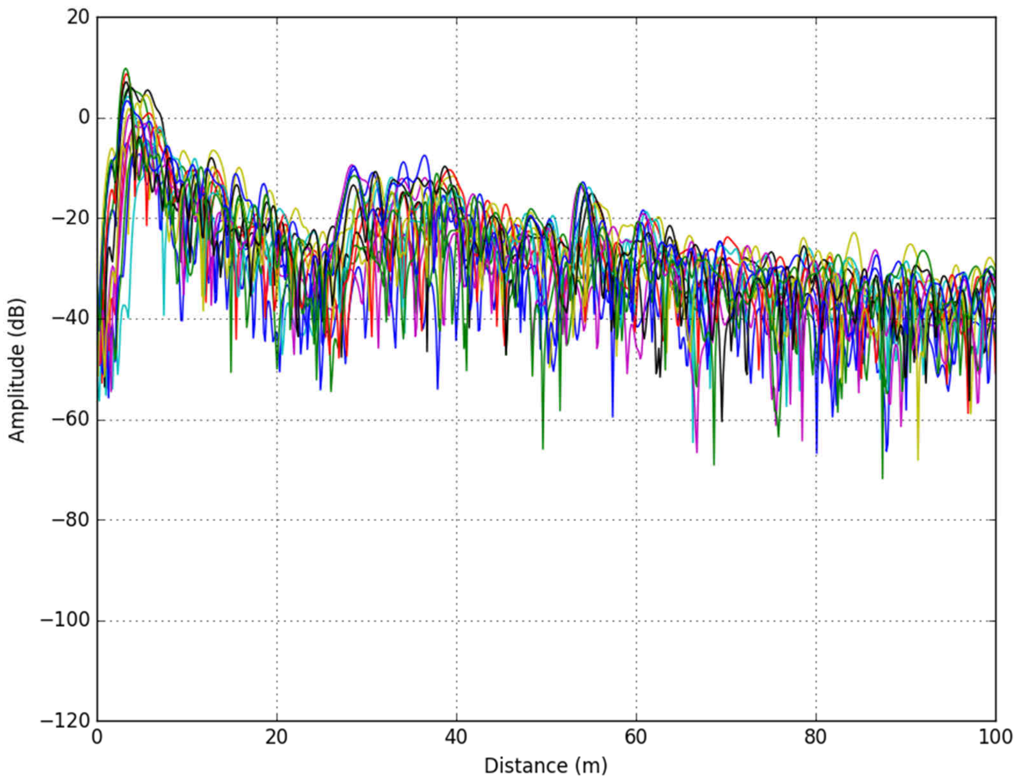

Figure 14: Impulse response of forest with corner reflector (HH polarisation) for the whole set of antennas couples; P band; HH polarisation

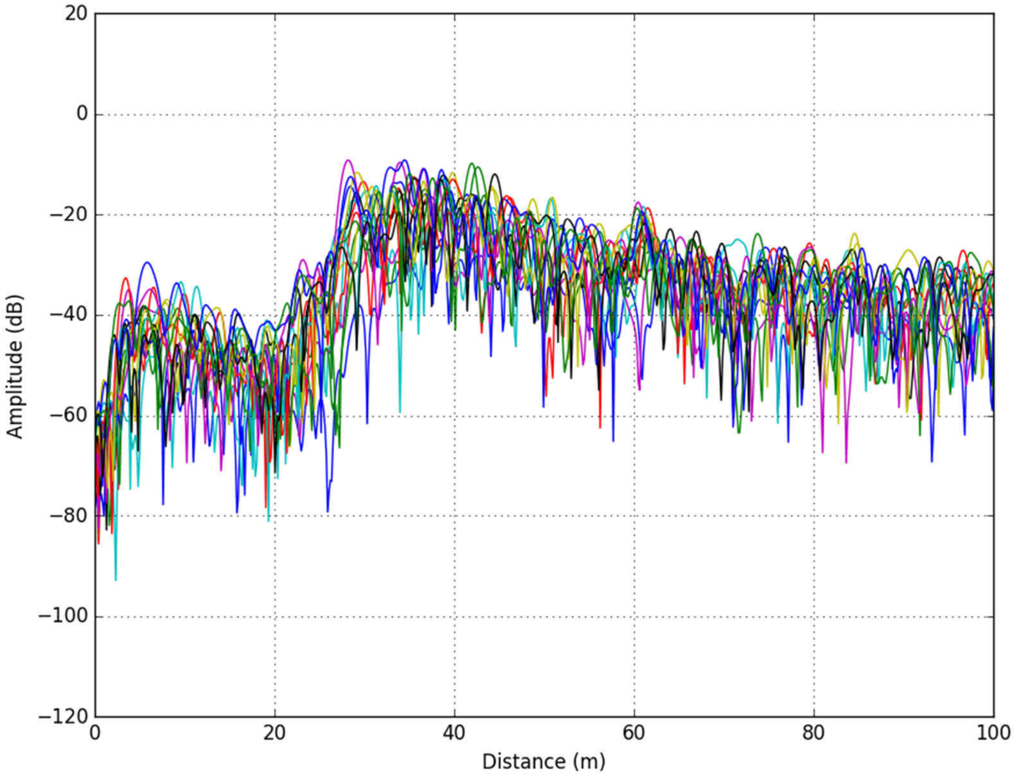

Figure 15: Impulse response of forest with corner reflector (HH polarisation) with chamber correction (forest alone) for all antenna pairs

To further qualify the system, data are processed with 2D tomography as shown in Figure 16 and Figure 17. The matched filter algorithm is applied to the data directly in the frequency domain. Note the results are weighted by the inverse of the antennas gain to really account for radar cross section which induces that in the useless parts of the image the spurious noise is amplified. Nevertheless one can see clearly in Figure 16 the diffracting points corresponding to the volume and the ground, the former being brighter the than the latter, the ground nadir echo and the CR exactly at the location expected. With chamber removal the CR appears more clearly, some strong scatterers are damped and most ground echoes, including the nadir one, are also damped. This experiment is a validation of the system well functioning since it proves all the coherency of phases of the system.

This ‘thriedral’ corner reflector was found to exhibit fair polarimetric expected properties after all corrections: HH~VV, HV less than 15 dB to HH and VV. It is taken as a calibrator in the following, especially in tomography which permits better isolating the CR from the background forest.

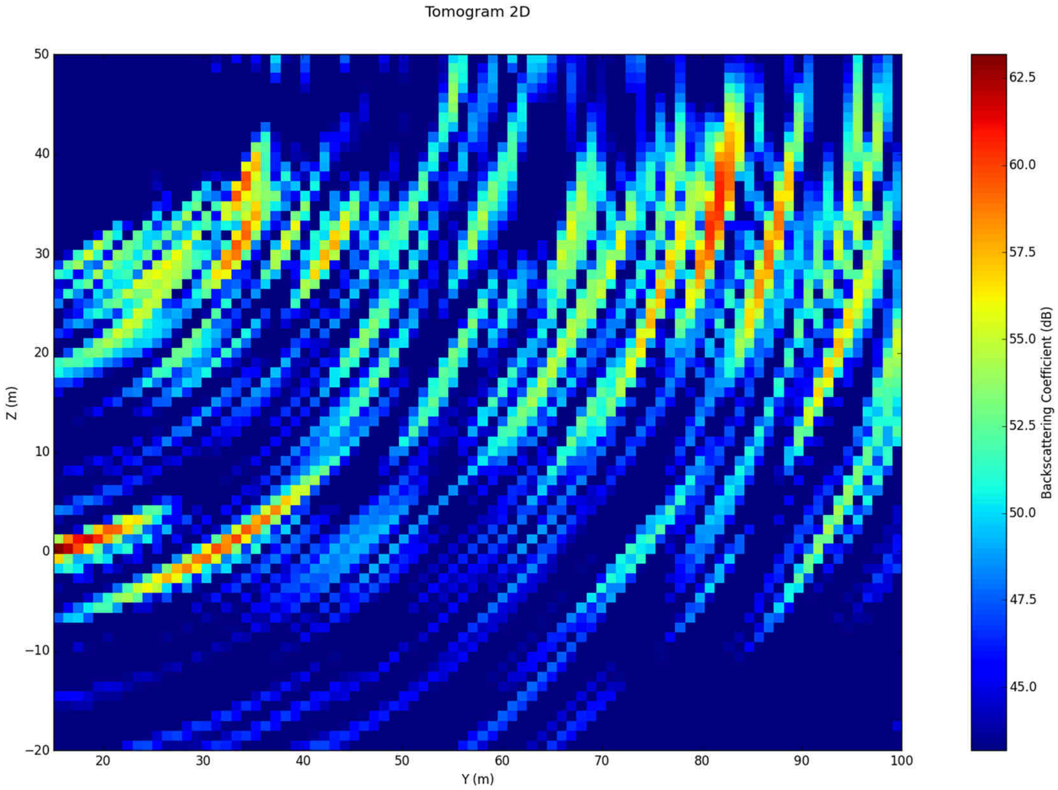

Figure 16 :2D tomographic image of forest with corner reflector (HH polarisation)

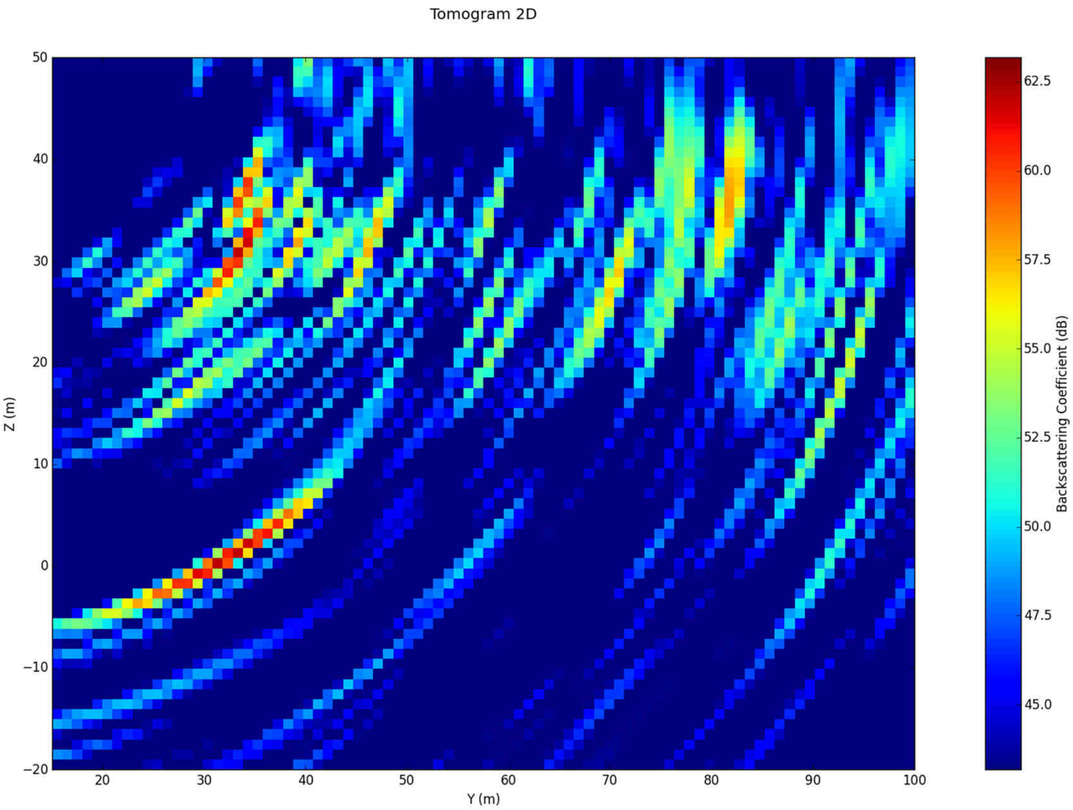

Figure 17 : 2D tomographic image of forest with corner reflector (HH polarisation) and chamber correction

3.3.2. SYSTEM COHERENCE

To check the system performances it is important to test the coherence of the system itself. For this we considered the coherent part of the impulses responses which corresponds to the coupling between the antennas which in principle should remain constant. The tower part may be affected all kind of changes, in particular the rain. The coherence is computed with considering several range gates of the impulse responses at the coupling distance for each antenna pair. It was found that all antennas work wery well in dry conditions in P and L bands, with logically better performances in P band and that with rain these performances are degraded for some antenna pairs, especially at L Band. Note that for Afriscat, with respect to Tropiscat, the antennas have been modified so that the influence of water on them is shorter after rain

To better qualify the system coherence, on can compute it computed over all the antenna pairs and also as a function of the temporal baseline. This is the system coherence and it will be accounted further for evaluating the forest one. It is displayed in Figure 18 and Figure 19 for P band at respectively rainy and dry season and in Figure 20 and Figure 21 for L band. In all cases, system coherence is better than 0.98 at P band and than 0.95 at L band.

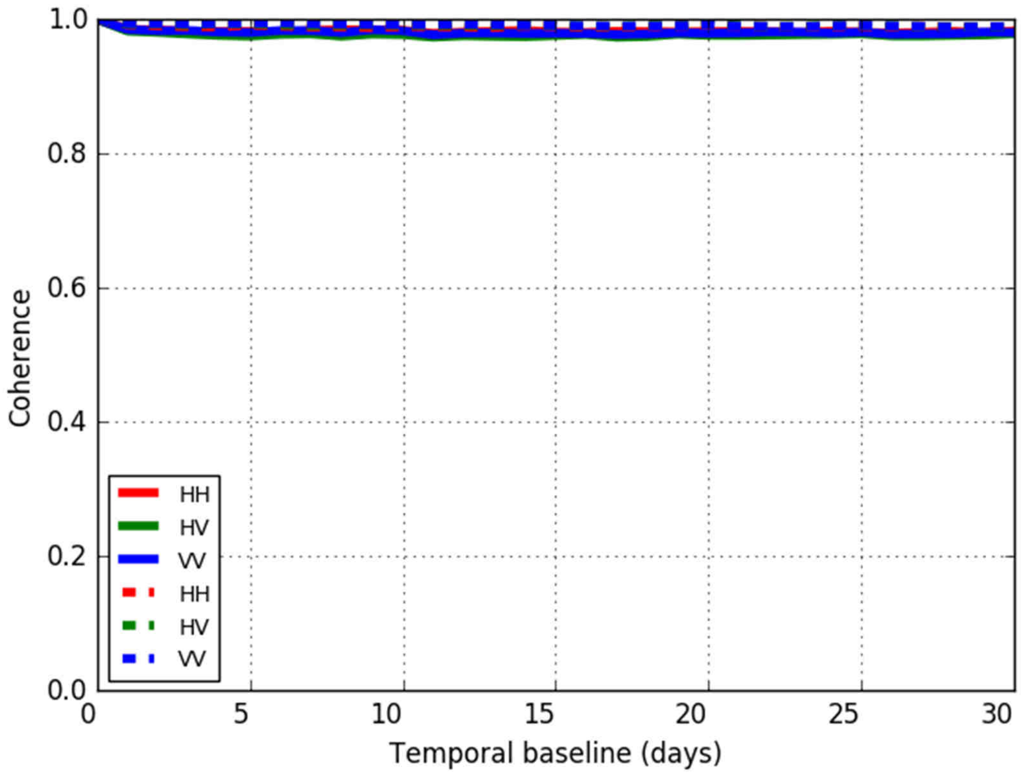

Figure 18 : System coherence vesus temporal baseline ; P band ; rainy season (from 2015/09/18 up to 2015/11/26). Full line at 6 am and dot line at 6 pm.

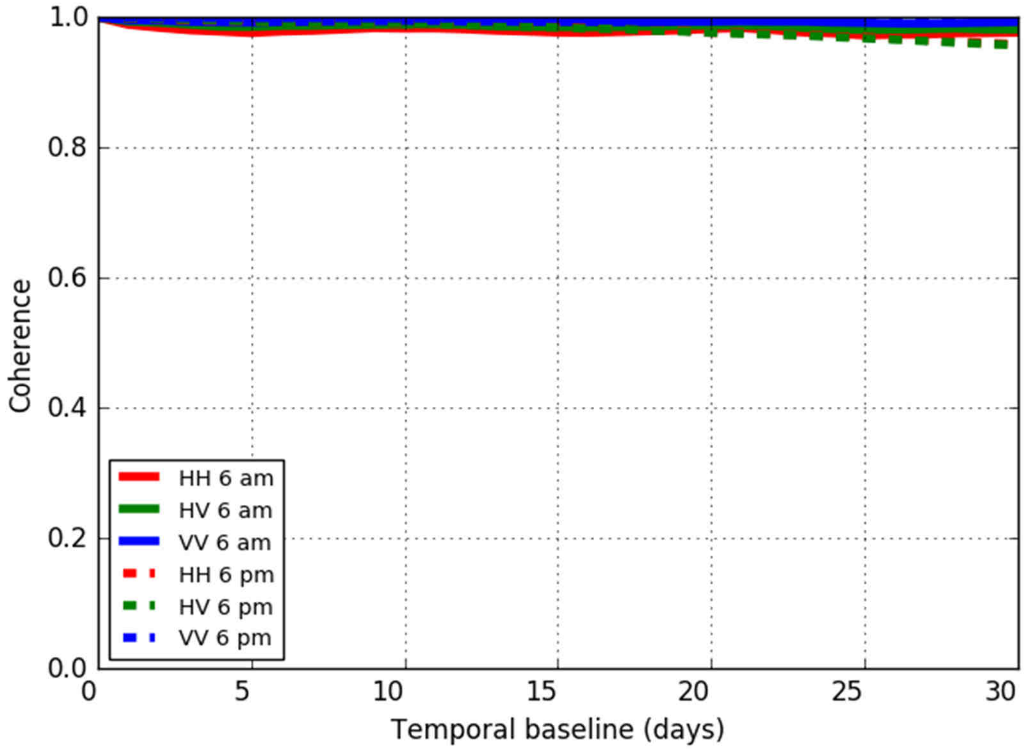

Figure 19 : System coherence vesus temporal baseline ; P band ; dry season (from 2015/11/27 up to 2016/02/04 à 6 am et 6 pm). Full line at 6 am and dot line at 6 pm.

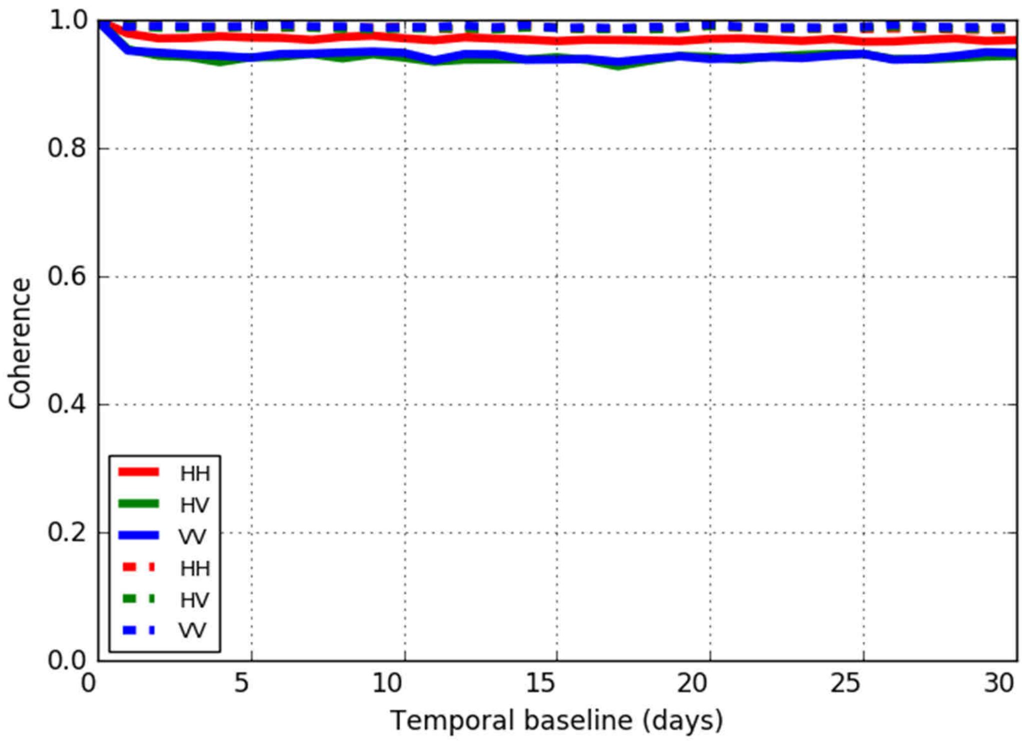

Figure 20 : System coherence vesus temporal baseline ; L band ; rainy season (from 2015/09/18 up to 2015/11/26). Full line at 6 am and dot line at 6 pm.

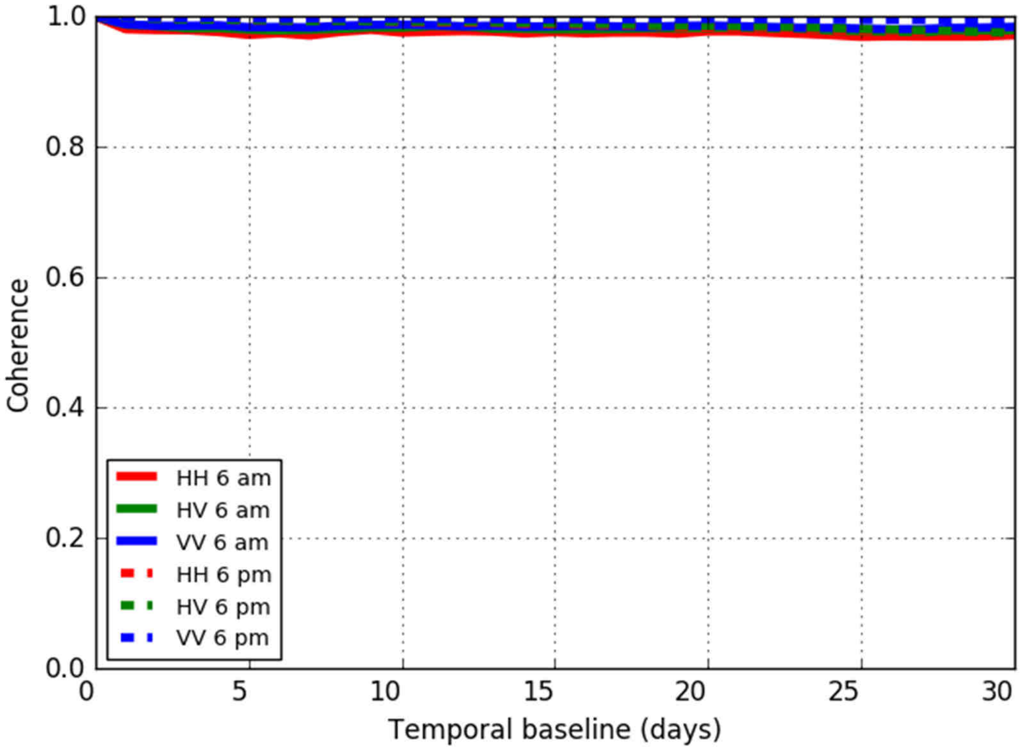

Figure 21: System coherence vesus temporal baseline ; L band ; dry season (from 2015/11/27 up to 2016/02/04). Full line at 6 am and dot line at 6 pm.

4. DATA ACQUISITION

4.1. ACQUISITION PLAN

To be in accordance with the electrical power capacity of the tower, the instrument was not running in 24h/24 mode. Power consumption budget allows running only 6 hours per day. To fit the BIOMASS requirements, the instrument was programmed be switched on 2 x 3 hours per day, i.e. 4:30-7h30 and 16:30-19h30 periods (local hours).

During these periods, the instrument followed this acquisition plan:

- 10 minutes cycle:
  - Band 1 (400MHz-600MHz):
    - Acquisition on calibration cable
    - Backscattering acquisitions (17 couples of antennas / polarisation)
      - R1T1, R1T2, R1T3, R1T5, R2T1, R2T2, R2T3, R2T5, R3T1, R3T2, R3T3, R3T5, R4T2 ,R4T3 ,R4T4 ,R5T5 ,R5T4 (all for HH,HV,VH and VV polarizations)
    - Acquisition on short circuit
  - Band 3 (800MHz-1GHz):
    - Acquisition on calibration cable
    - Backscattering acquisitions (17 couples of antennas / polarisation)
      - R1T1, R1T2, R1T3, R1T5, R2T1, R2T2, R2T3, R2T5, R3T1, R3T2, R3T3, R3T5, R4T2 ,R4T3 ,R4T4 ,R5T5 ,R5T4 (all for HH,HV,VH and VV polarizations)
    - Acquisition on short circuit

This plan is illustrated on Figure 22.

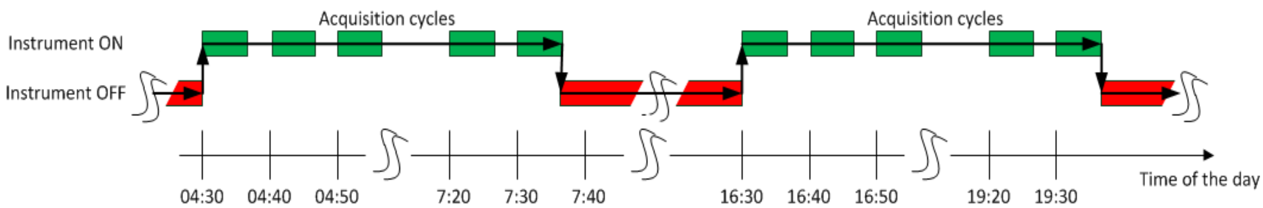

Figure 22 - Instrument acquistion plan

4.2. DATA LIST

The instrument has been running from July 2015 to December 2016. The following graph shows the data available on the acquisition period.

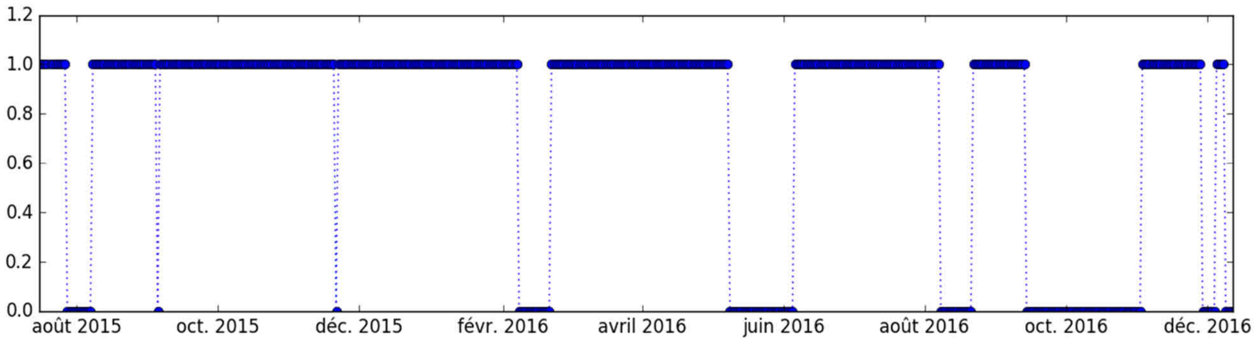

Figure 23 - Data available (1=data ; 0= no data)

The missing data are mainly due to electrical power failure.

4.3.IN-SITU DATA

In situ data was collected from the tower equipement. They include air temperature, rain fall, soil moisture.

Technical problems with the power unit and the acquisition system explain the missing data during some periods.

This table shows the rain fall difference between Paracou et Ankasa. We can notice that Ankasa is a dryer area than Paracou during the experiment.

Mean/SD Rainfall	Paracou { daily mean ; SD }	Ankasa { daily mean ; SD }
Dry	{ 38/65d=0.58mm ; 2.32mm }	{ 16.4/69j=0.24mm ; 0.87mm }
Rainy	{ 1577/100d=15.8mm ; 20.94mm }	{ 352.5/70=5mm ; 8mm }

5. DATA PROCESSING AND ANALYSIS

In this chapter, we explain the principle of data processing needed to analyze the temporal coherence and the intensity of the backscattering data.

5.1. OVERVIEW OF DATA PROCESSING

The measurement are performed by the VNA in the frequency domain. Then they have to be transformed into the time domain or equivalent range domain by IFFT (Inverse Fast Fourier Transform). So, for each acquisition we obtain a complex impulse response. If Δf and ∂f are respectively the frequency bandwidth and the frequency step, with $\Delta f = (Nf - 1) \times \partial f$, then the range resolution is $dr = \frac{c}{2\Delta f}$ and the unambiguous range $D = \frac{c}{2\partial f}$. So, for the range $i.dr$, the range profile is defined by the complex array $S(i)_t = \left(X(i)_t, Y(i)_t\right)$ where "i" is the i_{th} range bin, and dr is the width of range bin.

The raw data must be processed before use for temporal coherence estimation. First, the antenna gain is accounted for.

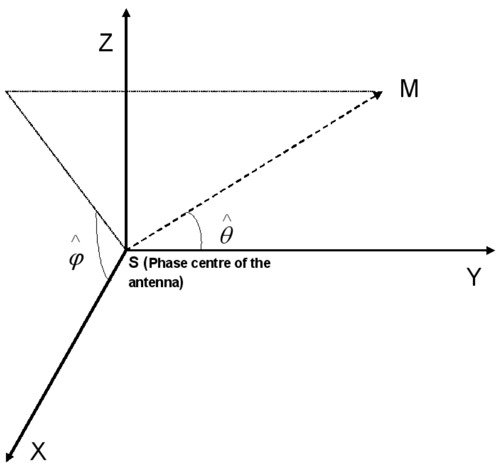

Figure 24: Coordinate system of the antenna

Figure 24 represents the coordinate system of the antenna $(SXYZ)$, $\hat{\theta}$ and $\hat{\varphi}$ are respectively the elevation and the azimuth angle. Considering Figure 24, the plane $\hat{\varphi} = \frac{\Pi}{2}$ is the elevation plane and $\hat{\varphi} = 0$ is the azimuth one.

The gain in the coordinate system of the antenna is given by Equation 1.

$$G'\left(\hat{\theta}, \hat{\varphi}\right) = G_{\max} - 3\frac{\hat{\theta}^2}{\theta_3^2}$$

Equation 1

Where $G_{\max}$ represents the maximum gain of the antenna and θ_3 corresponds to 3 dB aperture and it is given by Equation 2

$$\theta_3 = \theta_{3elev}.\cos^2\left(\hat{\varphi} - \frac{\pi}{2}\right) + \theta_{3az}\sin^2\left(\hat{\varphi} - \frac{\pi}{2}\right)$$

Equation 2

Where θ_{3elev} corresponds to 3 dB aperture in the H plane for H polarisation and in the E plane for V polarisation, whereas θ_{3az} corresponds to 3 dB aperture in the H plane for V polarisation and in the E plane for H polarisation.

On the other hand, in the coordinate system $(Oxyz)$ tied to the soil as horizontal plane (Oxy) and to the tower axis (Oz), an observation point M is in spherical coordinates defined by (r, θ, φ). These coordinates depend on $\hat{\theta}$ and $\hat{\varphi}$ as follows (Equation 3):

$$\cos\hat{\theta} = \sin\theta\sin\varphi\sin\theta_0 + \cos\theta\cos\theta_0$$

$$\cos\hat{\varphi} = \frac{\sin\theta\cos\varphi}{\sin\hat{\theta}}$$

$$\sin\hat{\varphi} = \frac{\sin\theta\sin\varphi\cos\theta_0 - \cos\theta\sin\theta_0}{\sin\hat{\theta}}$$

Equation 3

Where θ_0 is the direction of maximum radiation, θ and φ are respectively the elevation and the azimuth angle in the $(Oxyz)$ coordinate system (Figure 25:).

As the presence of the corner reflector may disturb the forest response, its measurements have been done at particular time slots with locating it on the forest ground with a quite clear line of sight from the tower top. Its contribution was evaluated with time gating and clutter removal with complex subtraction which appeared to be fully efficient for more than 30 minutes.

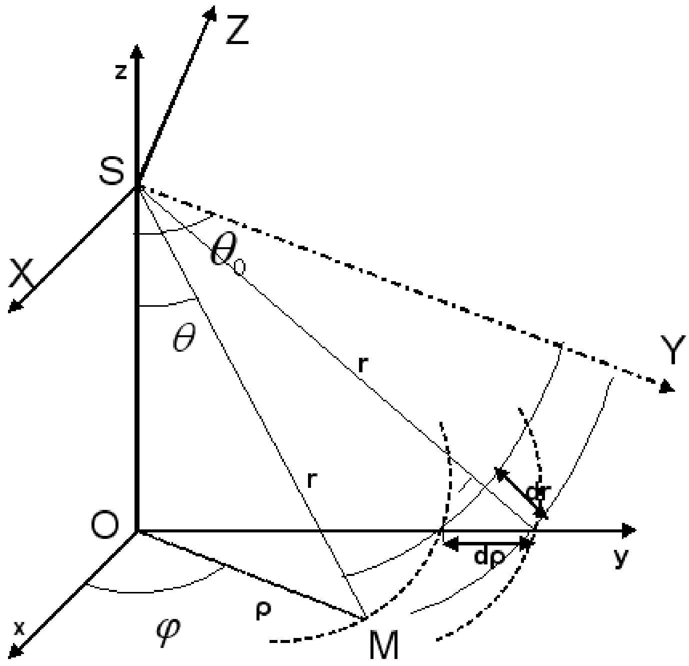

Figure 25: Antenna-ground geometry and illuminated surface projected on ground

For the forest, it is to evaluate the weighted illuminated area I_{pq} for a given range cell.

Let $G(\theta,\varphi) = G'\left(\hat{\theta},\hat{\varphi}\right)$

$$I_{pq} = \int_{\varphi=0}^{\varphi=\pi} G_e(\theta,\varphi).G_r(\theta,\varphi)\rho d\rho d\varphi = \int_{\varphi=0}^{\varphi=\pi} G'_e\left(\hat{\theta}(\theta,\varphi),\hat{\varphi}(\theta,\varphi)\right)G'_r\left(\hat{\theta}(\theta,\varphi),\hat{\varphi}(\theta,\varphi)\right)rdrd\varphi$$

Equation 4

As $\rho d\rho = rdr$,with ρ the distance from the soil to the bottom tower axis,

and with $p = \left|{}^{H}_{V}\right.$ and $q = \left|{}^{H}_{V}\right.$, G_e the emission gain, G_r the reception gain.

Note that it was delicate to position the trihedral reflector because of the forest presence. So this introduces some uncertainty related to the calibration. Or this point is not critic because only a relative calibration is required here to perform temporal monitoring. However, such calibration allows normalization between polarizations and antennas pairs.

Another correction was made in order to adjust the impulse response. In fact, it was noted that the direct coupling between antennas may be subject to some changes with time in particular during the rainy period. However this direct coupling is supposed to be constant. Consequently, we have established a method to adjust data that corrects this effect and normalize the level of direct coupling between antennas at a constant level. In fact, the hypothesis that a change in the antenna gain is fully characterized by the coupling change is done.

To do this, an impulse response measured at dry time is chosen and considered as a reference $S'_{ref} = \left(X'_{ref}, Y'_{ref}\right)$. All impulse responses include the antennas direct coupling, the tower coupling and the forest response as displayed in (Figure 26:).

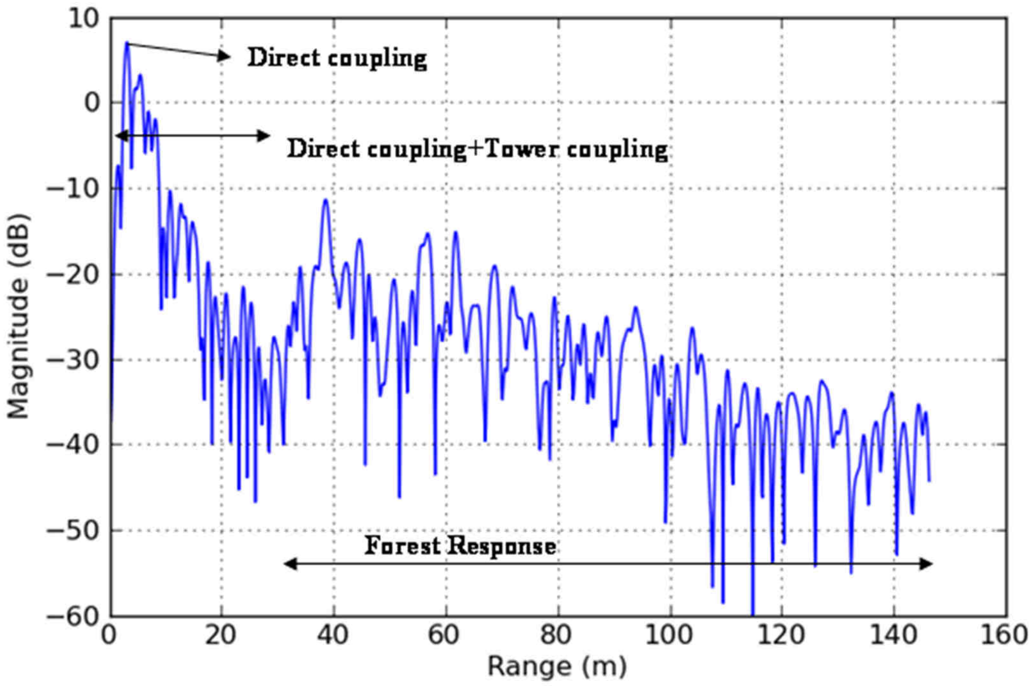

Figure 26: The backscattered impulse response

For all impulse responses $S'(i)_t = (X'(i)_t, Y'(i)_t)$, the real and imaginary parts are corrected as follows:

$$X_{pqt}(i) = X'_{pqt}(i).\frac{C_{pqref}}{C_{pqt}} \qquad \text{and } Y_{pqt}(i) = Y'_{pqt}(i).\frac{C_{pqref}}{C_{pqt}}$$

Equation 5

Where, by averaging the power around the direct coupling peak over N cells, we have:

$$C_{pqref} = \sqrt{\frac{\sum_{i\max-\Delta Ni/2}^{i\max+\Delta Ni/2}\left(X'^{\,2}_{pq\,ref} + Y'^{\,2}_{pq\,ref}\right)}{N}} \quad ; \quad C_{pqt} = \sqrt{\frac{\sum_{i\max-\Delta Ni/2}^{i\max+\Delta Ni/2}\left(X'^{\,2}_{pq_t} + Y'^{\,2}_{pq_t}\right)}{N}}$$

Equation 6

where $p = \left|{}^{H}_{V}\right.$, $q = \left|{}^{H}_{V}\right.$, $i_{\max}$ is the index of coupling peak, Δ_i is the number cells around the $i_{\max}$, $N = \Delta N_i + 1$.

Furthermore, it was noted that the direct coupling between antennas can be subject to changes during the rainy period. We have established a method to correct this effect by normalizing the level of direct coupling between antennas at the same level as a reference level chosen in the dry period [Hamadi et al., 2013a] and [Hamadi et al., 2013b].

5.1.1. TEMPORAL COHERENCE COMPUTATION

The temporal coherence is an indicator of the change in forest backscattering between two measurements made at two different times. The short-term variations are due to the wind movement, rain fall, soil moisture and long-term variations include the growth of the forest, cumulative rain fall, vegetation and soil moisture... In this section, we study the variations of the temporal coherence at different time scales and assess the link of these variations to the weather parameters which are wind speed and rain fall.

Considering simultaneously K antenna pairs illuminating the same range gate, the temporal complex coherence coefficient between the backscattered signals S_2 at t2 andS_1 at t1 is given by Équation 1.

$$\gamma_{pq} = \frac{\sum_{k=1}^{K} \sum_{i\min}^{i\max} S_{1\ pq}^{k}(i).\, S_{2\ pq}^{k}(i)^{*}}{\sqrt{\sum_{k=1}^{K} \sum_{i\min}^{i\max} \left|S_{1\ pq}^{k}(i)\right|^{2} \sum_{k=1}^{K} \sum_{i\min}^{i\max} \left|S_{2\ pq}^{k}(i)\right|^{2}}}$$

Équation 1

with $p = \left| {}^{H}_{V} \right.$ and $q = \left| {}^{H}_{V} \right.$, $i_{\min}$ and $i_{\max}$ correspond to the limits of the range gate under consideration, k refers to the considered antenna pair, K is the total number of antenna pairs taken in consideration. Actually, in Équation 1, the range cells of the impulse responses several antenna pairs' are combined and incorporated in a single complex vector. The time interval t2-t1 is the temporal baseline. In the following, coherence will refer to the modulus of the complex coherence coefficient.

To obtain a good estimation of the coherence, a minimum number of independent looks is necessary [Touzi et al., 1999]. This number can be provided by the number of spatial resolutions within the measured area, and also by the number of antenna pairs. An increasing number of antenna pairs was tested. To assess the stability of the measurements, we choose a spatial zone limited between 45 m to 60 m starting from the tower basis, corresponding to an incidence angle on the forest of about 44°. Within this area, there are 15 range cells of the size of spatial resolution (about 1m including the apodization factor) per antenna pair.

5.1.2. BACKSCATTERING COEFFICIENT COMPUTATION

As mentioned above, for each acquisition we obtain a normalized range backscattering profile and for the range $i.dr$, the range profile is defined by the complex array $S(i)_t = \left(X(i)_t, Y(i)_t\right)$. The backscattering coefficient I_{pq} is computed by averaging the backscattering coefficient range profile in distance, time and several couples successively. First, we define a range gate for filtering the data. At a given time t (iteration time, every 15 mn), we perform an averaging over resolution cells (Equation 7)

$$I_{pq}(t,c) = \frac{\sum_{r=r\min}^{r\max} \left(X(r)^2 + Y(r)^2\right)}{N_r}$$

Equation 7

Where c defines a couple of antennas, t is the time of acquisition and r a given range cell. Nr is the number of cells between $r_{\min}$ and $r_{\max}$.

Then an averaging temporal window Δt is defined and the backscattering coefficient is computed with the following averaging, with N_T the number of acquisitions (Equation 8):

$$I_{pq}(t,c) = \frac{\sum_{t'=t-\Delta t/2}^{t+\Delta t/2} I_{pq}(t',c)}{N_T}$$

Equation 8

with $p = \begin{vmatrix} H \\ V \end{vmatrix}$ and $q = \begin{vmatrix} H \\ V \end{vmatrix}$

Finally, for increasing the degree of liberty and increasing the number of computational cells we performed an averaging over several couples (Equation 9). In fact, the behaviour of the backscattering coefficient changes according to the considered couple: each couple sees a different scene. So using several antennas increases the number of independent looks.

$$I_{pq}(t) = \frac{\sum_{c=1}^{Nc} I_{pq}(t,c)}{N_c}$$

Equation 9

Where Nc is the number of couples.

5.2.STATISTICAL ANALYSIS OF TEMPORAL COHERENCE

With the time series of backscattering coefficients, we can compute the coherence and the backscaterring intensity change for all date couples (temporal baseline). A matrix representation of these data can beused, as displayed in Figure 27. The upper diagonal is for the coherence values between pairs, and the lower diagonal part for the differential backscaterring defined by one minus the normalized difference between backscattering coefficients at 2 dates..

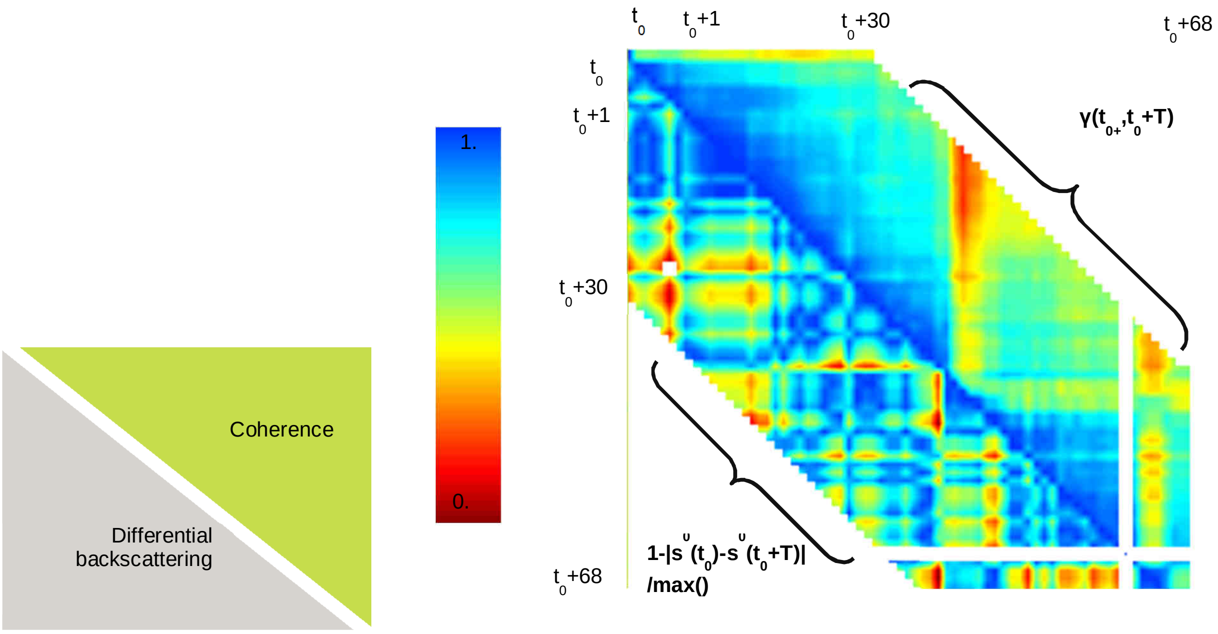

Figure 27 : Coherence and backscattering intensity matrix

Such representation enables to visualize all possible combinations of pairs, and particularly the most impacted by changes whether on the coherence or on the backscatter. For these specific dates, it is interesting to see if lower coherences are associated to a higher differential backscattering, and to see the symmetry or not with past and future acquisitions.

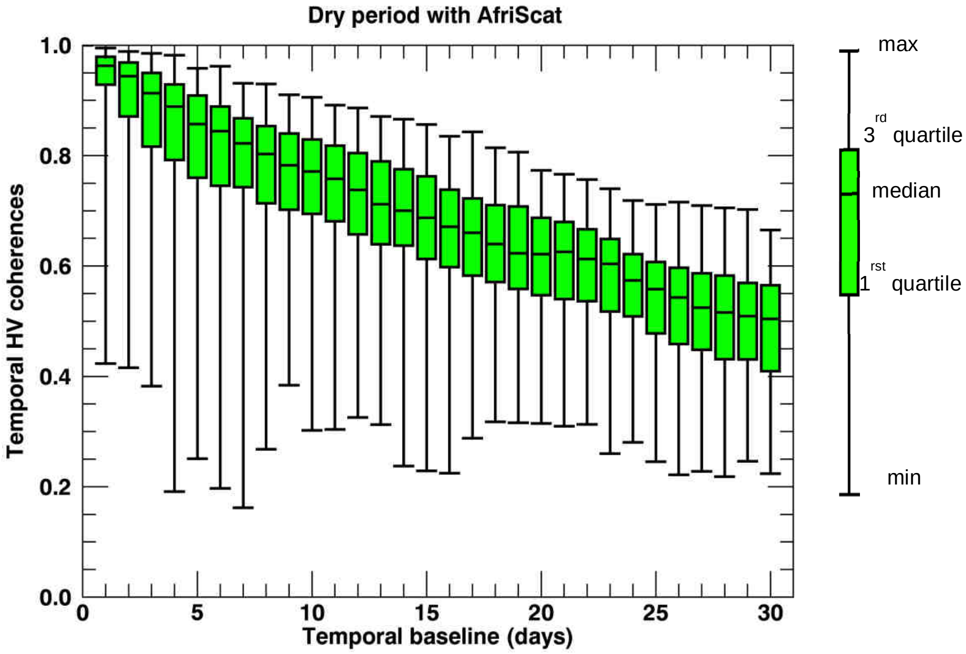

Figure 28 - Example of box-and-whisker coherence plots as a function of temporal baseline, in which the first and third quartiles define the box boundaries with the median in between, and the whiskers are for the minimum and maximum values among all the pairs that correspond to a given temporal baseline.

5.2.1. STATISTICAL DISTRIBUTIONS VS TEMPORAL BASELINE

To characterize the coherence distributions versus the temporal baseline, we consider the following subsets of acquisitions:

- between 5h30 and 6h30 am or 5h30-6h30 pm,
- with spatial range 45-60 m to keep incidence angle as closed as possible to the BIOMASS configuration.

For each temporal baseline between 1 and 30 days and the above subsets, a distribution of coherences can be obtained.

The following graphs represent these distributions for HH, HV and VV polarizations during the dry and wet seasons.

		
HH	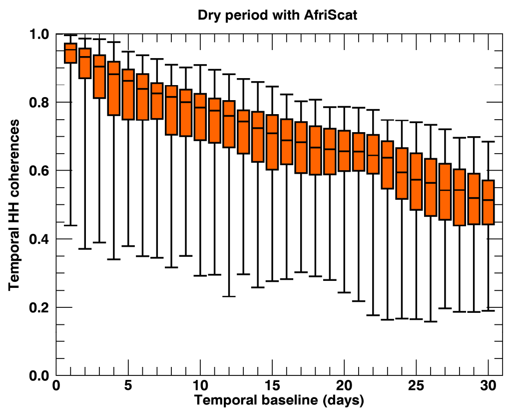	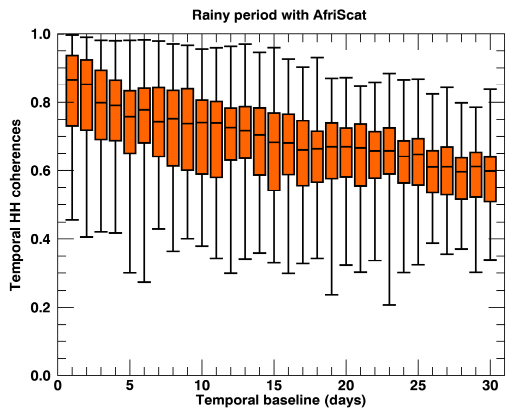
HV	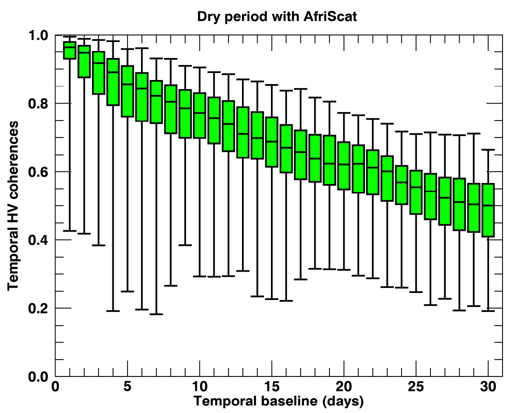	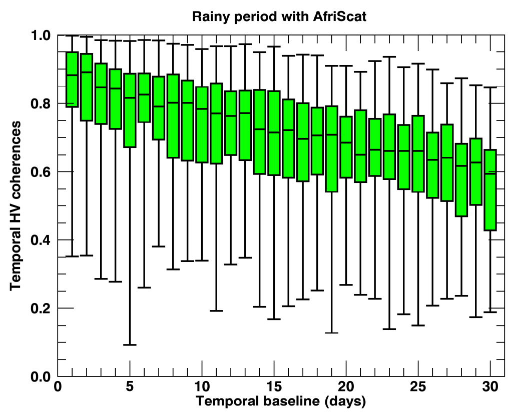

VV

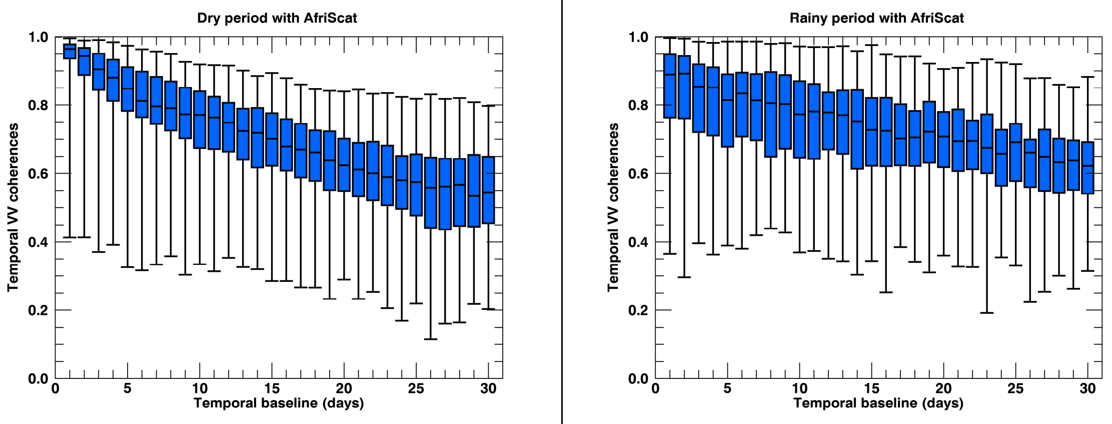

Figure 29 : Box-and-whisker coherence plots as a function of temporal baseline, as explained in Figure 27. Left and right columns are respectively for the dry and rainy seasons, while each line is for the indicated polarization.

Box-and-whisker coherence plots in Figure 29 show that all the 3 polarizations behave similarly for a given season (dry or rainy). As expected, short term decorrelation (at 1 day) is stronger during the rainy season, given that the rainy events come mostly with wind turbulences. Considering a temporal baseline of 3 days (as scheduled for the Biomass mission), the coherences are higher than 0.9 half of the time during the dry season, and higher than 0.85 during the rainy one. However, these graphs also show that there is a risk of 75% to deal with coherences lower that 0.8 and 0.7 during the dry and rainy seasons respectively.

More surprising between the dry and rainy seasons is the fact that decorrelation becomes stronger during the former after about 10 days, with a median value of about 0.8 for both cases. Indeed, we can also stress the fact that the decorrelation patterns between the two seasons are very different, the decreasing trend being quite linear during the rainy season, whereas there is a kind of drop after 1 day during the rainy season followed by a quasi linear trend with a lower slope than . As a consequence, the two patterns intersect (around 10 days), and at 30 days the coherences are significantly higher during the rainy season (median above 0.6 against 0.5).

Further analysis are needed to strengthen the possible explanations, among which the fact that the vegetation (and particularly its water content) evolves more rapidly during the dry season is for us the most likely, as observed with the diurnal cycles that are much less accentuated during rainy days.

5.2.2. PROBABILITIC ANALYSIS

From the coherence distribution, we can now estimate the probability to get a coherence value greater than a given threshold.

The following graphs represent these probabilities for HH, HV and VV polarizations during the dry and wet seasons.

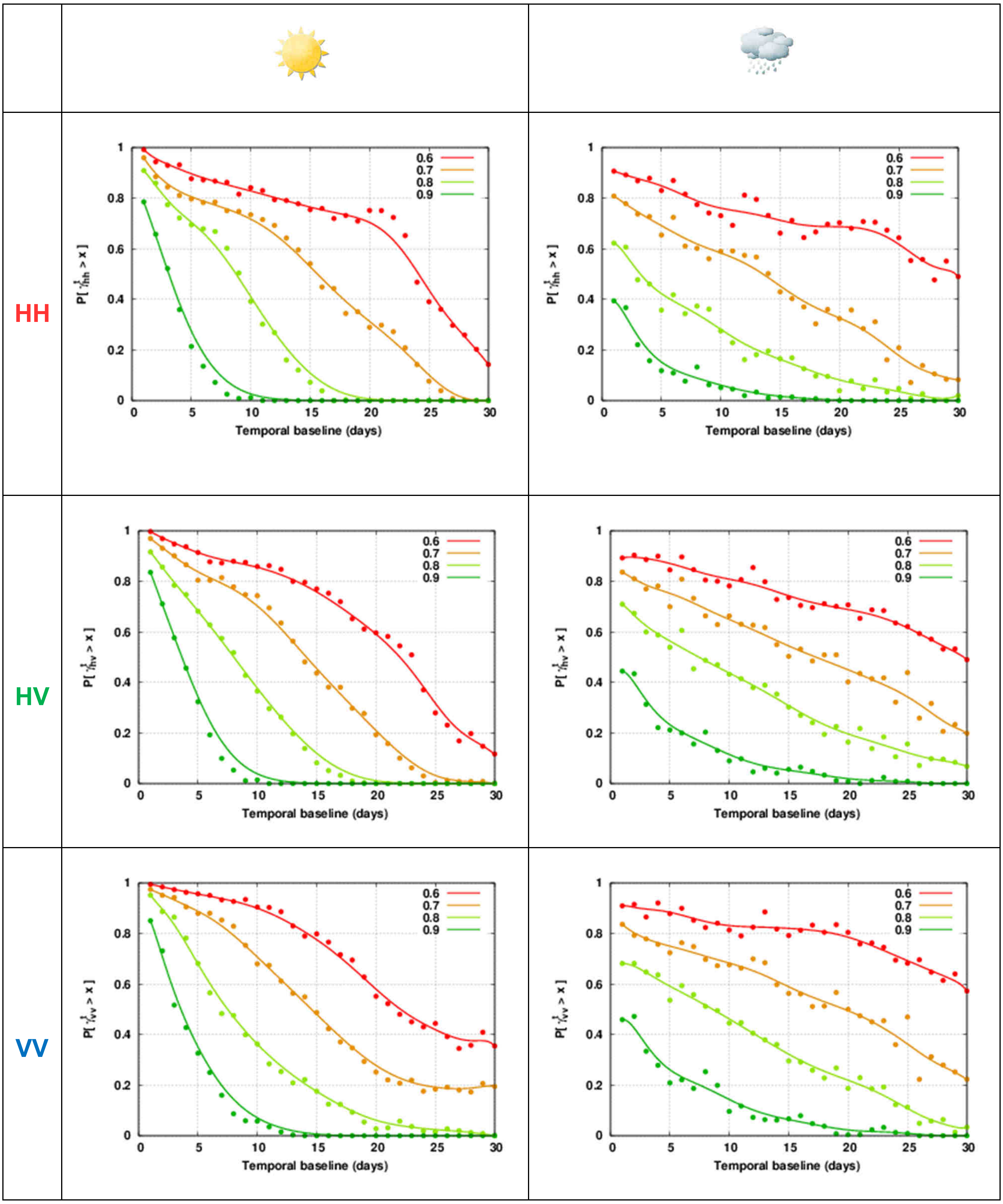

Figure 30: Probabilities to get coherences higher than the indicated thresholds in the subcaption (0.6,0.7,0.8,0.9) as function of the temporal baseline between a single pair. As displayed before, left and right columns are respectively for the dry and rainy seasons. The fitting lines are derived from Bezier curves.

From the afore-mentioned coherence distributions, various probability calculations can be performed in a mission scenario frame. As an example, we can see from the curves in Figure 30 show that the probabilities to get coherences from a given pair during the dry season higher than 0.9 and after 3 days is around 0.5 (as shown before by the box-and-whiskers plots), but the same probability in the rainy season is only around one third.

5.2.3. IMPACT OF ACQUISITION TIME (6 AM/PM)

The previous results have been derived from acquisitions within the 5h30-6h30 am slot, which can be compared to the 5h30-6h30 pm slot as shown in Figure 31.

For most cases (polarization and temporal baselines), probabilities to get coherences above the chosen thresholds are significantly significantly higher with am acquisitions. In agreement with previous analysis from the TropiScat data, this result confirms that acquisitions during the morning are less impacted by decorrelation caused by convective wind turbulences, that remain non negligible after the noon peak.

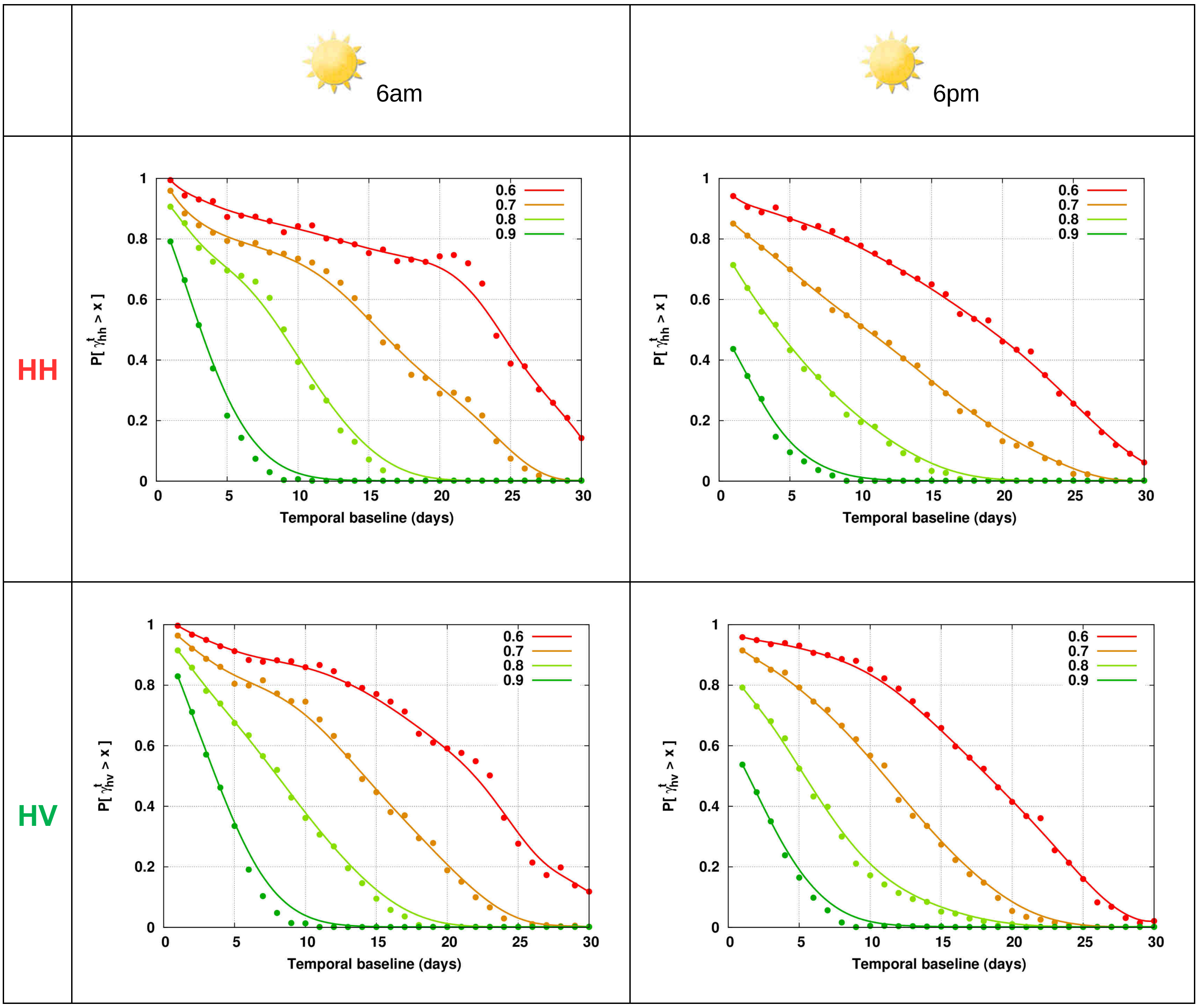

VV

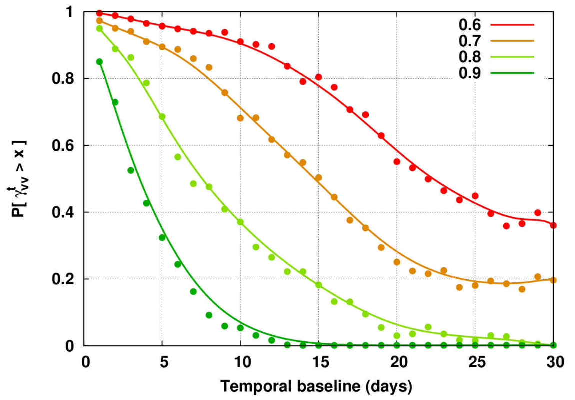

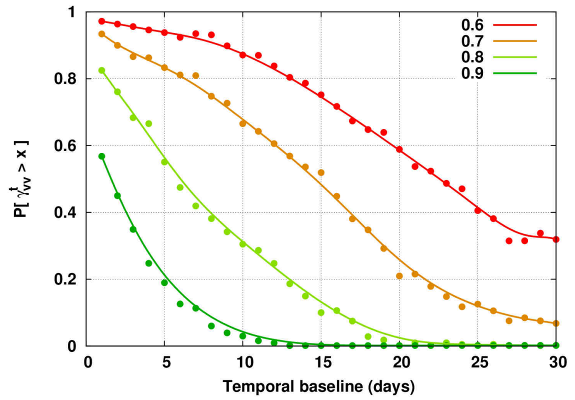

Figure 31 : Probabilities to get coherences higher than the indicated thresholds in the subcaption (0.6,0.7,0.8,0.9) as function of the temporal baseline between a single pair. Left and right columns are respectively for acquisitions within the 5h30-6h30 am and pm slots.

5.2.4. PROBABILISTIC ANALYSIS ON BIOMASS SCENARIO

In the BIOMASS mission scenario, we want to get at least one pair (optimal for PolInSAR) with γ(t,t+3) > [0.8,0.9] with N acquisitions (from AfriScat statistical results at 6 am +/- 30min, for dry & rainy periods)

HH

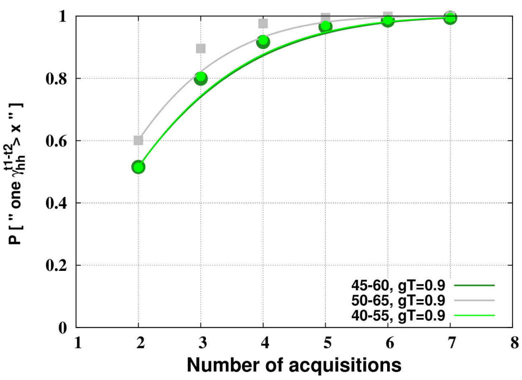

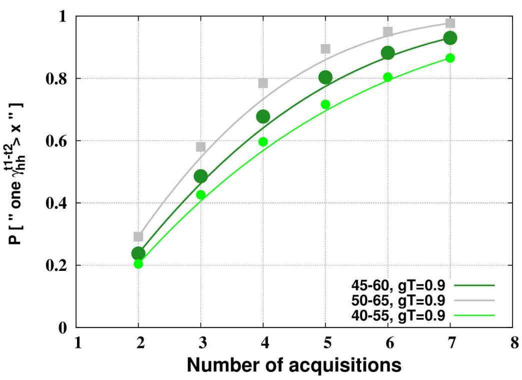

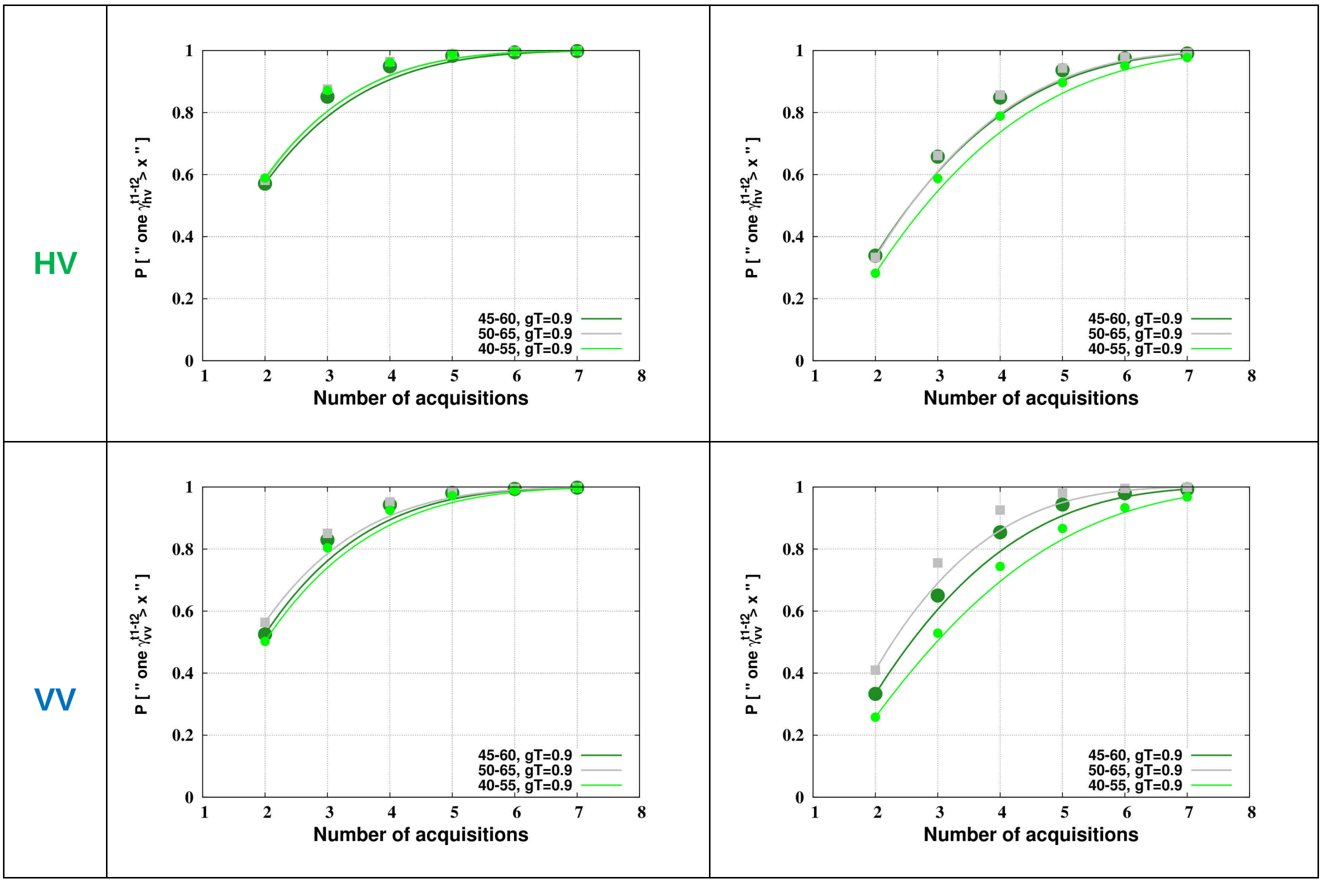

Figure 32 : Probabilities to get from N acquisitions (from 2 to 7 along the abscissa axis) one pair with a coherence higher than 0.9. Left and right columns are respectively for acquisitions within the 5h30-6h30 am slots for the dry and the rainy periods. The three fitting curves of sets of points are for several ranges within the instrument swath.

In the frame of Biomass mission Tomographic or Interferometric phases, a number of 3 to 7 pairs will be available.

Considering the backup possibility during both phases to exploit at least one of these acquisitions, the probability to have at least on pair almost free of temporal decorrelation (above 0.9) can be derived, as shown in Figure 32 as a function of the number of acquisitions.

For all cases, it is interesting to note the significant gain from 2 to 5 acquisitions before reaching values close to the maximum. It can be also stressed that with the 7 tomographic phase acquisitions it is almost always possible to have at least one pair with a coherence higher than 0.9, except for HH during the rainy season and the two nearest ranges.

We also add that testing the various ranges within the instrument swath enable to see the stability of the results according to slight changes of acquisition geometry and forest structure.

5.3.TEMPORAL VARIATIONS OF BACKSCATTERED INTENSITIES

We can also analyse the temporal variation of the intensity of the backscattering. Figure 33 and Figure 34 represents respectively the intensity during the dry and the rainy seasons.

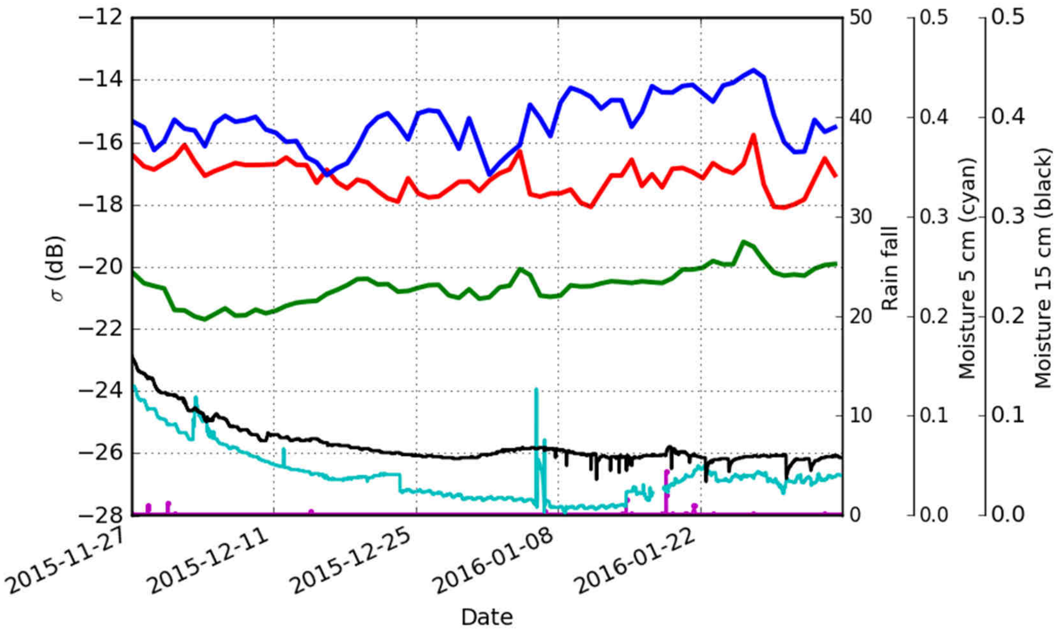

Figure 33 – Temporal intensity variation at 6am during the dry season.
Red (HH) ; Green (HV) ; Blue (VV)
Black : soil moisture @ 5 cm ; Cyan : soil moisture @ 15 cm ; Purple : Rain fall

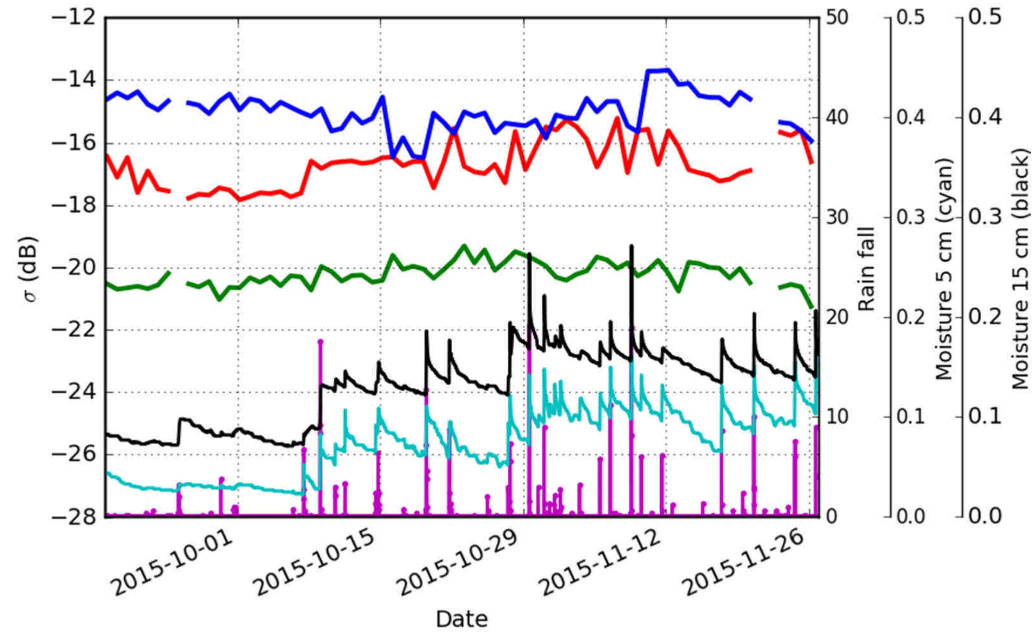

Figure 34 – Temporal intensity variation at 6am during the rainy season.
Red (HH) ; Green (HV) ; Blue (VV)
Black : soil moisture @ 5 cm ; Cyan : soil moisture @ 15 cm ; Purple : Rain fall

5.3.1. STATISTICAL ANALYSIS OF BACKSCATERRING INTENSITIES

Considering all the data acquired during the campaign, we can compute the distribution of the intensity. As the variation of the intensity (along time) is more relevant than the intensity value itself, we can plot the difference in dB of the intensity between two acquistion separed of the baseline. Figure 35 illustrates these resultats for all polarizations and for the two seasons.

<table>
<tr><td></td><td></td><td></td></tr>
<tr><td>HH</td><td>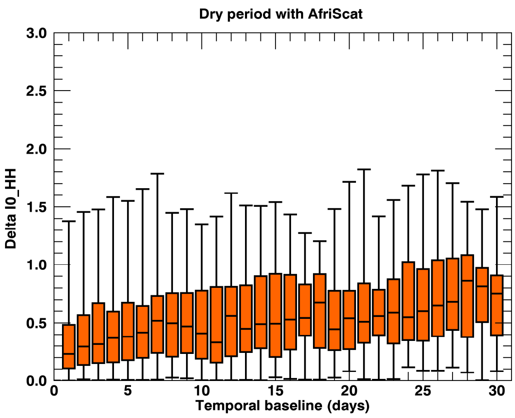
</td><td>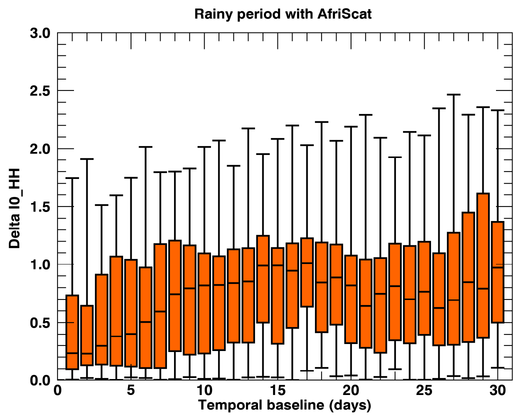
</td></tr>
<tr><td>HV</td><td>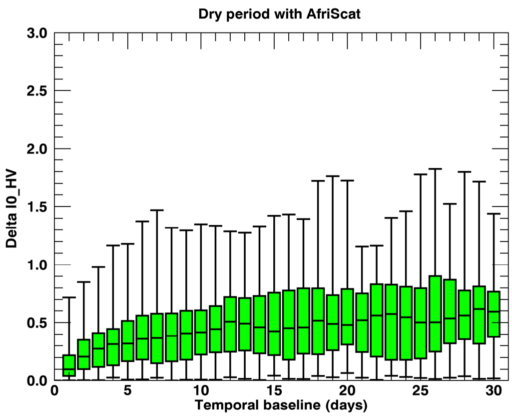
</td><td>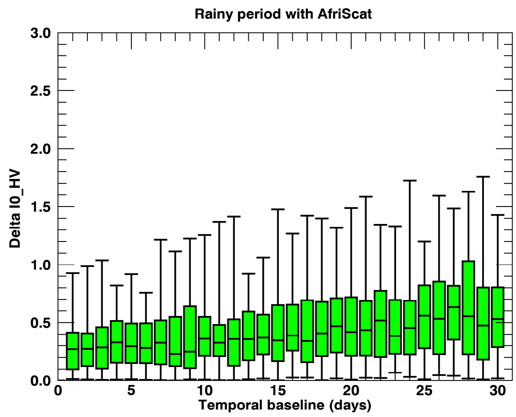
</td></tr>
</table>

VV	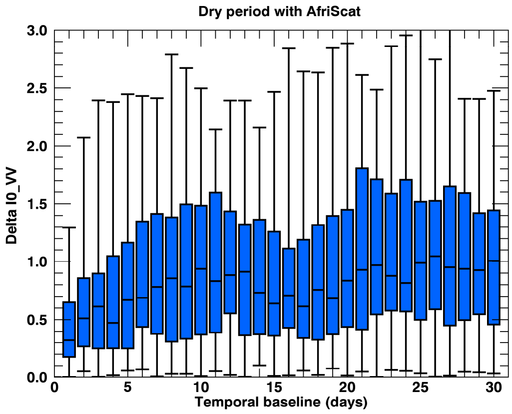	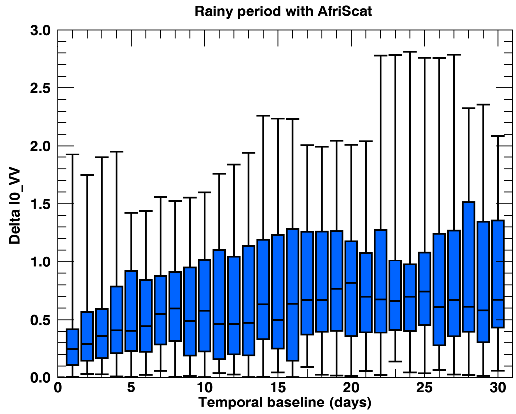

Figure 35- Box-and-whisker intensity variation plots as a function of temporal baseline. Left and right columns are respectively for the dry and rainy seasons, while each line is for the indicated polarization.

6. DATA FORMAT

The data are delivered in two different datasets.

6.1.RAW DATASET

This dataset contains the data directly from the VNA. No processing is done.

It consists in a set of ASCII files (CSV format). Each file represents one acquisition (backscaterring coefficient) in frequency domain. The filename follows the convention:

ANK_Yyyyy**-M**mm**-D**dd_hh**H**mm_**I**iiiii_**BAND**b_pp_**R**r_**T**t**.CSV**

yyyy is the year of acquisition (2015-2016)

mm is the month of acquisition (01-12)

dd is the day of acquisition (01-31)

iiiii is the index number of the acquisition

b is the band number (1 = 400-600 MHz and 3 = 800-1000 MHz)

pp is the polarization (HH,HV,VV,VH)

r is the antenna number in reception (1-5)

t is the antenna number in transmit (1-5)

Each file is written in the following format:

```
"# Channel 1"
"# Trace 1"
Frequency, Formatted Data, Formatted Data
+4.00000000000E+008, +5.85200906274E-006, -4.97869198200E-006
+4.00125000000E+008, -9.76936928414E-006, +1.39484332933E-005
+4.00250000000E+008, -1.98403551726E-005, -4.80100963040E-006
+4.00375000000E+008, +1.25050729583E-005, -1.91097065708E-005
…
```

It consists in 1601 lines (one per frequency), containing 3 floats (frequency in Hz, real and imaginary parts of backscaterring coefficient)

6.2.NETCDF DATASET

Raw data have been pre-processed to generate a netCDF dataset. It consists in a set of files (one file per day).

This dataset include both frequency domain data (like raw dataset) and distance domain data.

The distance domain data is computed by applying a Hamming window before the Fourier transform.

The netCDF format is following:

```
netcdf Y2016-M02-D12_B3 {
types:
  compound complex {
    float real ;
    float imag ;
  }; // complex
dimensions:
	nb_points = 1601 ;
	nb_antennas = 17 ;
	time = UNLIMITED ; // (0 currently)
	nb_dist_points = 4096 ;
variables:
	string time_of_the_day(time) ;
		time_of_the_day:format = "hhHmm" ;
	float frequency(nb_points) ;
		frequency:long_name = "Frequency" ;
		frequency:valid_min = 0.f ;
		frequency:valid_max = 1.e+09f ;
		frequency:unit = "Hz" ;
	string antenna_pairs(nb_antennas) ;
		antenna_pairs:long_name = "Antenna pair" ;
		antenna_pairs:unit = "Rx_Ty" ;
	complex HH(time, nb_antennas, nb_points) ;
		HH:long_name = "Complex backscaterring coefficient in HH" ;
		HH:unit = "" ;
	complex HV(time, nb_antennas, nb_points) ;
		HV:long_name = "Complex backscaterring coefficient in HV" ;
		HV:unit = "" ;
	complex VH(time, nb_antennas, nb_points) ;
		VH:long_name = "Complex backscaterring coefficient in VH" ;
		VH:unit = "" ;
	complex VV(time, nb_antennas, nb_points) ;
		VV:long_name = "Complex backscaterring coefficient in VV" ;
		VV:unit = "" ;
	float distance(nb_dist_points) ;
		distance:long_name = "Distance" ;
		distance:valid_min = 0.f ;
		distance:valid_max = 600.f ;
		distance:unit = "meters" ;
	complex HH_distance(time, nb_antennas, nb_dist_points) ;
		HH_distance:long_name    =    "Distance-domain    complex    backscaterring
coefficient in HH" ;
		HH_distance:unit = "" ;
	complex HV_distance(time, nb_antennas, nb_dist_points) ;
		HV_distance:long_name    =    "Distance-domain    complex    backscaterring
coefficient in HV" ;
		HV_distance:unit = "" ;
	complex VH_distance(time, nb_antennas, nb_dist_points) ;
		VH_distance:long_name    =    "Distance-domain    complex    backscaterring
coefficient in VH" ;
		VH_distance:unit = "" ;
	complex VV_distance(time, nb_antennas, nb_dist_points) ;
		VV_distance:long_name    =    "Distance-domain    complex    backscaterring
coefficient in VV" ;
		VV_distance:unit = "" ;
```

```
// global attributes:
              :_NCProperties                                                              =
"version=1|netcdflibversion=4.4.1.1|hdf5libversion=1.8.18" ;
              :history = "none" ;
              :campaign = "Afriscat" ;
              :title = "Complex Backscattering coefficients" ;
              :acquisition_date = "Yyyyy-Mmm-Ddd" ;
              :product_version = "1.0" ;
              :contact = "thierry.koleck@cesbio.cnes.fr" ;
              :file_quality_index = 1. ;
              :frequency_band = "BAND1" ;
}}
```

6.3. IN-SITU DATA

In situ data are given in a self-content Excel file.

7. REFERENCES

[1] «Tropiscat Final Report,» 2014.

[2] A. L. J. B. P. V. R. Touzi, «Coherence estimation for SAR Imagery,» *IEEE Transactions on Geoscience and Remote Sensing,* vol. 37, n° %11, pp. 135-149, 1999.